NASA
Technical
Paper
2604

September 1986

Effects of Model Error on Control of Large Flexible Space Antenna With Comparisons of Decoupled and Linear Quadratic Regulator Control Procedures

Harold A. Hamer and
Katherine G. Johnson

NASA

NASA Technical Paper 2604

1986

Effects of Model Error on Control of Large Flexible Space Antenna With Comparisons of Decoupled and Linear Quadratic Regulator Control Procedures

Harold A. Hamer and
Katherine G. Johnson

Langley Research Center
Hampton, Virginia

National Aeronautics
and Space Administration

**Scientific and Technical
Information Branch**

Summary

An analysis has been performed to determine the effects of model error on the control of a large flexible space antenna. Control was achieved by employing two three-axis control-moment gyros (CMG's) located on the antenna column. State variables were estimated by including an observer in the control loop that used attitude and attitude-rate sensors on the column. Errors were assumed to exist in the individual model parameters: modal frequency, modal damping, mode slope, and moment of inertia. Their effects on control-system performance were analyzed either for (1) nulling initial disturbances in the rigid-body modes, or (2) nulling initial disturbances in the first three flexible modes. The study includes the effects on stability, time to null, and control requirements (defined as maximum torque and total momentum), as well as on the accuracy of obtaining initial estimates of the disturbances. The effects on the transients of the undisturbed modes are also included. The results, which are compared for decoupled and linear quadratic regulator (LQR) control procedures, are shown in tabular form, parametric plots, and as sample time histories of modal-amplitude and control responses.

Results of the analysis showed that the effects of model errors on the control-system performance were generally comparable for both control procedures. The effect of mode-slope error was the most serious of all model errors.

Introduction

Large space structures (LSS) will require control for attitude orientation as well as procedures for controlling the flexible modes. After deployment or construction, any control required will most likely be performed with a control procedure based on inaccurate knowledge of model parameters. There are many identification and adaptive control procedures that have been developed (for example, ref. 1) for updating and verifying these parameters. However, the practical application of these procedures for operation in space has not been fully tested. Hence, a considerable period of time may be required before a more accurate model can be determined. Consequently, a knowledge of the effects of model errors on the stability and control requirements for LSS control would be useful.

The effects of model errors are addressed in the present paper with regard to the control of a 122-m-diameter hoop-column antenna (ref. 2). A finite-element mathematical model of the antenna is used that provides a convenient tool for simulated control analysis of realistic large flexible space structures. Previous control studies that used this antenna model include references 3 to 5. The antenna is depicted in sketch A and is described in reference 2.

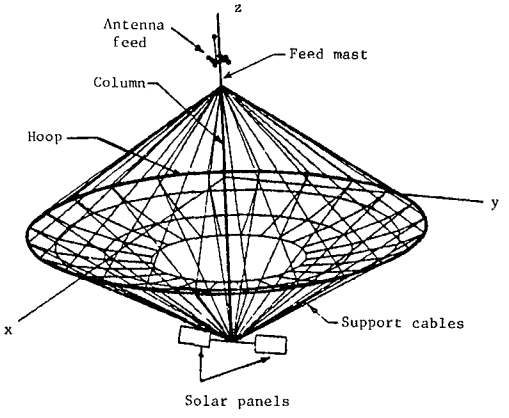

Sketch A

The present paper is based on the control analysis reported in reference 4. In this reference an observer was used for estimating the state variables for control feedback. In addition, residual modes were included in the antenna model and the effects of including these modes were investigated. The control arrangement employed one three-axis control-moment gyro (CMG) at the top of the antenna column and one at the bottom. Only the first three flexible modes were included in the control law, inasmuch as data in reference 3 showed large increases in the control requirements with additional modes included. In reference 4 it was shown that decoupled and linear quadratic regulator (LQR) control procedures gave comparable results; hence, the effects of model errors for both procedures are analyzed and compared in the present analysis.

Errors are assumed to exist in the individual model parameters: modal frequency, modal damping, mode slope (control-influence coefficient), and moment of inertia. Their effects on control-system performance are analyzed either for (1) nulling initial disturbances in the rigid-body modes, or (2) nulling initial disturbances in the first three flexible modes. The study includes the effects on stability, time to null, and control requirements (defined as maximum torque and total momentum), as well as on the accuracy of obtaining initial estimates of the disturbances. The effects on the transients of the undisturbed modes are also included. Results are shown in tabular form, parametric plots, and as sample time histories of modal-amplitude and control responses. For the analysis, random positive and negative errors

were incorporated into the frequency and mode-slope parameters, as were certain errors in the damping and moment of inertia; their effects were analyzed individually for specified magnitudes of error. The analyses were carried out for a large number of samples in order to obtain the maximum effects of these errors. The control system and observer were assumed to be perfect in that no actuator or sensor dynamics were included in the analysis.

Symbols and Abbreviations

$\mathbf{A}$	system matrix (eq. (4))
A_n	modal amplitude (eq. (2)), where n is mode number (1,2,...,6)
$\mathbf{B}$	control influence matrix (eq. (4))
$\mathbf{C}$	observation matrix (eq. (9))
CMG	control-moment gyro
$\mathbf{d}$	displacement vector (eq. (3))
$\mathbf{F}$	decoupled feedback gain matrix (eq. (5))
$\mathbf{G}$	decoupled feedforward gain matrix (eq. (5))
$\mathbf{I}$	moment-of-inertia matrix (eq. (1))
I	model moment of inertia
I_x, I_y, I_z, I_{xz}	center-of-gravity moments and product of inertia
J	objective function (eq. (7))
$\mathbf{K}$	LQR feedback gain matrix (eq. (6))
$\mathbf{K}'$	estimator gain matrix (eqs. (13))
LQR	linear quadratic regulator
l	distance (see fig. 1)
$M_{i,j}$	angular momentum, where i is control direction and j is actuator location
M_N	nominal total momentum (no model error)
M_ϵ	total momentum with model error
$\mathbf{Q}$	state-vector weighting matrix (eq. (7))
$\mathbf{R}$	control-vector weighting matrix (eq. (7))
r	radius of hoop
$\mathbf{s}$	vector of system input noise (eq. (10))
$\mathbf{T}$	torque vector
$T_{i,j}$	components of torque, where i is control direction and j is actuator location
$T_{\max}$	maximum value for actuator requiring largest torque
T_N	nominal $\lvert T_{\max}\rvert$ (no model error)
T_n	natural period
T_ϵ	$\lvert T_{\max}\rvert$ with model error
t	time
$\mathbf{u}$	vector of observation noise (eq. (8))
$\mathbf{v}$	input command vector (eq. (5))
w	weight
$\mathbf{x}$	state vector
$\hat{\mathbf{x}}$	estimate of controlled state vector
x, y, z	coordinates of antenna center of gravity
$\mathbf{y}$	observation vector (eq. (8))
$\mathbf{z}$	sensor output vector without noise
ϵ	estimator error, $\mathbf{y} - \mathbf{C}'\hat{\mathbf{x}}$
ς_d	desired damping ratio
ς_n	natural damping ratio
θ, ϕ, ψ	rotation angle about x-, y-, and z-axis, respectively
$\mathbf{\Phi}$	mode-shape matrix (eq. (3))
$\mathbf{\Phi}'^{(n)}_{i,j}$	mode-slope matrix, where n is mode number, i is control direction, and j is actuator location
ω_d	desired frequency
ω_n	natural frequency

Subscripts:

A_n	modal amplitude for nth mode
i, j	control direction and actuator location, respectively
θ, ϕ, ψ	rotation angle about x-, y-, and z-axis, respectively

A matrix with a prime relates to the estimator equations. Dots over symbols indicate derivatives with respect to time. A circumflex ($\hat{}$) over a symbol indicates an estimate of the state variable. All matrices are given in units of inches, pounds, and seconds.

Mathematical Model of Antenna

A large space structure such as the hoop-column antenna has, in theory, an infinite number of flexible (vibration) modes. To facilitate analytical treatment of the control problem, a finite-order linearized model was formulated. For the analysis of this report, the structural model was selected to contain six of the lowest flexible modes of the 122-m-diameter hoop-column antenna, as described in reference 2. The three rigid-body rotation modes are included in the analysis.

The equations of motion used to represent the rigid-body and vibration modes of the antenna are now discussed. Rigid-body rotations (for small angles) about the antenna center of gravity for two three-axis CMG actuators on the column are represented by

$$\begin{pmatrix} \ddot{\theta} \\ \ddot{\phi} \\ \ddot{\psi} \end{pmatrix} = \left[\mathbf{I}^{-1} \;\middle|\; \mathbf{I}^{-1} \right] \mathbf{T} \tag{1}$$

where

$$\mathbf{T} = [T_{x,1},\ T_{y,1},\ T_{z,1},\ T_{x,2},\ T_{y,2},\ T_{z,2}]^T$$

The CMG's were used on the column such that control torques were about the $x-$, $y-$, and $z-$axes as defined in figure 1. The CMG's are numbered to be consistent with reference 3.

Variations in modal amplitudes of the flexible modes are represented by

$$\ddot{A}_n + 2\zeta_n \omega_n \dot{A}_n + \omega_n^2 A_n = \frac{1}{m_n} \mathbf{\Phi}'^T \mathbf{T} \qquad (n = 1, 2, ..., 6) \tag{2}$$

where m_n is the modal mass and $\mathbf{\Phi}'$ is the mode-slope matrix. It should be noted that A_n values in equation (2) are modal-amplitude displacement variables and do not represent actual physical displacements. The physical displacement at some point on the antenna is a linear combination of the modal amplitudes and mode shapes and is given by the transformation

$$\mathbf{d}_j = \mathbf{\Phi} A_n \tag{3}$$

where $\mathbf{\Phi}$ is the mode-shape matrix.

The mode-slope data used in the analysis were taken from results of a NASTRAN® model of the 122-m-diameter hoop-column antenna system given in reference 3. Table I shows the weight and inertias of the antenna. The frequencies and assumed natural damping ratios of the six flexible modes considered in the analysis are also given in table I. As a matter of interest, the unforced transient behavior of these modes is presented in figure 2.

Decoupled and LQR Control

The second-order equations in the analysis (eqs. (1) and (2)) can be reduced to first-order equations (state-vector form) and written as

$$\dot{\mathbf{x}} = \mathbf{A}\mathbf{x} + \mathbf{B}\mathbf{T} \tag{4}$$

where the state vector

$$\mathbf{x} = [\theta,\ \phi,\ \psi,\ A_1,\ A_2,\ ...,\ A_6,\ \dot{\theta},\ \dot{\phi},\ \dot{\psi},\ \dot{A}_1,\ \dot{A}_2,\ ...,\ \dot{A}_6]^T$$

A_1, A_2, and A_3 are the controlled flexible modes, and A_4, A_5, and A_6 are considered as residual modes. The $\mathbf{B}$ matrix used in the present analysis is given in table AI in the appendix. The composition of the $\mathbf{A}$ matrix is defined as follows:

$$\mathbf{A}_{18\times 18} = \left[\begin{array}{c|c} \mathbf{0}_{9\times 9} & \mathbf{I}_{9\times 9} \\ \hline -\mathbf{\Lambda}_{9\times 9} & -\mathbf{D}_{9\times 9} \end{array} \right]$$

where the subscripts indicate the dimensions of the various elements, and

$\mathbf{0}$	null matrix
$\mathbf{I}$	identity matrix
$\mathbf{\Lambda}$	$\text{diag}(0,\ 0,\ 0,\ \omega_1^2,\ \omega_2^2,\ ...,\ \omega_6^2)$
$\mathbf{D}$	$\text{diag}(0,\ 0,\ 0,\ 2\zeta_1\omega_1,\ 2\zeta_2\omega_2,\ ...,\ 2\zeta_6\omega_6)$

Decoupled Control

Since decoupling theory was analyzed extensively in reference 3, the discussion of its application in

this paper is limited to some general remarks. The decoupling control law is taken as

$$\mathbf{T} = \mathbf{F}\hat{\mathbf{x}} + \mathbf{G}\mathbf{v} \tag{5}$$

where $\hat{\mathbf{x}}$ is the estimated state vector, $\mathbf{v}$ is the input command vector, and $\mathbf{F}$ and $\mathbf{G}$ are feedback and feedforward gain matrices, respectively. (As noted, estimates of the modal variables are employed because these variables cannot be measured directly.) Decoupling theory provides a method for determining the $\mathbf{F}$ and $\mathbf{G}$ matrices such that independent control is maintained for each of the decoupled (controlled) state variables. Different values can be selected for the closed-loop dynamics (ω_d and ς_d) without affecting the independent control capability. Examples are given in reference 3 that illustrate the manner in which the theory was applied to the system equations in determining the $\mathbf{F}$ and $\mathbf{G}$ matrices. The values for the decoupled closed-loop dynamics used in the current analysis are given in table II. This case corresponds to ς_d values that give approximately the same value (10 sec) for time to damp to 1 percent for each of the three flexible modes. The other case represents the closed-loop dynamics pertaining to the LQR control analysis, which are close to those for decoupled control. The corresponding $\mathbf{F}$ gain matrix used in the current analysis for decoupled control is given in table AII in the appendix. The $\mathbf{G}$ matrix, which is required for rigid-body commands, was not used in the present analysis. Rigid-body commands were not analyzed inasmuch as the results would be similar to those for the control for the rigid-body disturbances. The $\mathbf{F}$ matrix was calculated for a reduced-order model (no residual modes). Hence,

$$\hat{\mathbf{x}} = \left[\hat{\theta},\ \hat{\phi},\ \hat{\psi},\ \hat{A}_1,\ \hat{A}_2,\ \hat{A}_3,\ \dot{\hat{\theta}},\ \dot{\hat{\phi}},\ \dot{\hat{\psi}},\ \dot{\hat{A}}_1,\ \dot{\hat{A}}_2,\ \dot{\hat{A}}_3\right]^T$$

LQR Control

The asymptotic linear quadratic regulator (LQR) approach of reference 6 was also used to calculate the state feedback control gains. (A computer program is given in ref. 7 for performing these computations.) When comparing the LQR and decoupled-control procedures, it should be noted that the decoupled approach has advantages in some areas. For example, the decoupled feedback gains are computed in closed form and yield the exact desired closed-loop dynamics, whereas the LQR approach requires an inexact, time-consuming iterative solution to obtain approximate desired closed-loop dynamics. Also, the decoupled gains give a known transient response (for perfect state-variable estimates), as well as a steady-state response. Only the steady-state response is known by use of the LQR method.

The control law for the LQR results was given by

$$\mathbf{T} = \mathbf{K}\hat{\mathbf{x}} \tag{6}$$

The control gain matrix $\mathbf{K}$ was computed subject to the constraint of equation (4) such that the following function was minimized:

$$J = \lim_{t\to\infty} \int_0^t (\mathbf{x}^T\mathbf{Q}\mathbf{x} + \mathbf{T}^T\mathbf{R}\mathbf{T})\, dt \tag{7}$$

where $\mathbf{Q}$ and $\mathbf{R}$ are positive definite symmetric weighting matrices for the states and controls, which can be varied in order to achieve desired closed-loop dynamics. For the present analysis, the identity matrix used for $\mathbf{R}$ was found to be sufficient; the state-variable weighting matrix $\mathbf{Q}$ was adjusted to obtain a set of closed-loop dynamics close to that used for decoupled control. (See table II.) The corresponding $\mathbf{K}$ gains were used in the control procedure (eq. (6)) for the subsequent LQR control analysis. The weightings $\mathbf{Q}$ and the $\mathbf{K}$-gain matrix are given in table AIII in the appendix.

Incorporation of Observer

An observer was incorporated into the control procedures in order to calculate estimates of the state variables as required in equations (5) and (6). The Kalman-Bucy filter, which represents a systematic procedure for observer design, is used for obtaining these estimates. An attitude-measurement device (e.g., a star tracker) and a rate-measurement device (e.g., a rate gyro) were assumed to be present at certain locations on the column. The sensor output is given by

$$\mathbf{y} = \mathbf{z} + \mathbf{u} \tag{8}$$

where $\mathbf{z} = \mathbf{Cx}$ and $\mathbf{u}$ is the sensor noise, which is assumed to be 0 for this analysis. As an example, the observation matrix $\mathbf{C}$ is

$$\mathbf{C}_{6\times 18} = \left[\begin{array}{ccc|ccc} & & & & \boldsymbol{\Phi}'^{(1)}_{x,1} \;\; \boldsymbol{\Phi}'^{(2)}_{x,1} \cdots \boldsymbol{\Phi}'^{(6)}_{x,1} \\ & \mathbf{0}_{3\times 9} & & \mathbf{I}_{3\times 3} & \boldsymbol{\Phi}'^{(1)}_{y,1} \;\; \boldsymbol{\Phi}'^{(2)}_{y,1} \cdots \boldsymbol{\Phi}'^{(6)}_{y,1} \\ & & & & \boldsymbol{\Phi}'^{(1)}_{z,1} \;\; \boldsymbol{\Phi}'^{(2)}_{z,1} \cdots \boldsymbol{\Phi}'^{(6)}_{z,1} \\ \hline & \boldsymbol{\Phi}'^{(1)}_{x,4} \;\; \boldsymbol{\Phi}'^{(2)}_{x,4} \cdots \boldsymbol{\Phi}'^{(6)}_{x,4} & & & \\ \mathbf{I}_{3\times 3} & \boldsymbol{\Phi}'^{(1)}_{y,4} \;\; \boldsymbol{\Phi}'^{(2)}_{y,4} \cdots \boldsymbol{\Phi}'^{(6)}_{y,4} & & \mathbf{0}_{3\times 9} & \\ & \boldsymbol{\Phi}'^{(1)}_{z,4} \;\; \boldsymbol{\Phi}'^{(2)}_{z,4} \cdots \boldsymbol{\Phi}'^{(6)}_{z,4} & & & \end{array}\right] \tag{9}$$

and

$$\mathbf{x} = \left[\theta,\ \phi,\ \psi,\ A_1,\ A_2,\ ...,\ A_6,\ \dot{\theta},\ \dot{\phi},\ \dot{\psi},\ \dot{A}_1,\ \dot{A}_2,\ ...,\ \dot{A}_6\right]^T$$

The matrix $\mathbf{I}_{3\times 3}$ is the identity matrix and $\mathbf{0}_{3\times 9}$ is the null matrix. The superscripts on the mode slopes refer to the flexible-mode number, and the subscripts refer to the direction and location. For example, the subscript $x, 1$ refers to the mode slope in the x-direction at location 1 on the antenna column (fig. 1.) The observation matrix shown in equation (9) corresponds to a sensed attitude rate in the x-, y-, and z-directions at location 1 and to a sensed attitude in the x-, y-, and z-directions at location 4. Mode-slope values for various locations on the column are given in reference 3. The values corresponding to equation (9) are given in table AIV in the appendix.

The complete set of equations required for the control analysis becomes

$$\dot{\mathbf{x}} = \mathbf{Ax} + \mathbf{BT} + \mathbf{s} \tag{10}$$

where $\mathbf{s}$, the process noise, is assumed to be 0 for this analysis,

$$\mathbf{T} = \mathbf{K}\hat{\mathbf{x}} \quad \text{(for LQR control)} \tag{11a}$$

$$\mathbf{T} = \mathbf{F}\hat{\mathbf{x}} + \mathbf{Gv} \quad \text{(for decoupled control)} \tag{11b}$$

$$\mathbf{y} = \mathbf{Cx} \tag{12}$$

$$\dot{\hat{\mathbf{x}}} = \mathbf{A}'\hat{\mathbf{x}} + \mathbf{B}'\mathbf{T} + \mathbf{K}'(\mathbf{y} - \mathbf{C}'\hat{\mathbf{x}})$$

where

$$\dot{\hat{\mathbf{x}}} = (\mathbf{A}' - \mathbf{K}'\mathbf{C}' + \mathbf{B}'\mathbf{K})\hat{\mathbf{x}} + \mathbf{K}'\mathbf{Cx} \quad \text{(for LQR control)} \tag{13a}$$

$$\dot{\hat{\mathbf{x}}} = (\mathbf{A}' - \mathbf{K}'\mathbf{C}' + \mathbf{B}'\mathbf{F})\hat{\mathbf{x}} + \mathbf{K}'\mathbf{Cx} + \mathbf{B}'\mathbf{Gv} \quad \text{(for decoupled control)} \tag{13b}$$

The estimator equations (eqs. (13)) calculate the estimates of the state vector using the measurement $\mathbf{y}$ and the estimator gains $\mathbf{K}'$, which are determined by a steady-state Kalman-Bucy filter. If all six flexible modes are estimated, then $\mathbf{C}' = \mathbf{C}$. However, if the residual modes are not estimated, as in the present analysis, $\mathbf{C}'$

becomes a 6×12 matrix. In this case, the six columns that contain the $\Phi'^{(4)}$, $\Phi'^{(5)}$, $\Phi'^{(6)}$ information are eliminated. The estimator gains $\mathbf{K}'$ were calculated by the technique given in reference 7. In conjunction with the $\mathbf{C}'$ matrix, it should be emphasized that there are two differences between the $\mathbf{A}'$, $\mathbf{B}'$, and $\mathbf{C}'$ matrices and the $\mathbf{A}$, $\mathbf{B}$, and $\mathbf{C}$ matrices. First, the primed matrices are of lower order than the unprimed matrices since they do not include the residual modes. Second, the unprimed matrices represent the actual (true) model parameters as revised by the various model parameter errors that modified the nominally assumed values.

The set of composite equations used for the LQR-control analysis is

$$\begin{pmatrix} \dot{\mathbf{x}} \\ -- \\ \dot{\hat{\mathbf{x}}} \end{pmatrix} = \left[\begin{array}{c|c} \mathbf{A}_{18\times18} & \mathbf{B}_{18\times6}\mathbf{K}_{6\times12} \\ \hline \mathbf{K}'_{12\times6}\mathbf{C}_{6\times18} & \mathbf{A}'_{12\times12} - \mathbf{K}'_{12\times6}\mathbf{C}'_{6\times12} + \mathbf{B}'_{12\times6}\mathbf{K}_{6\times12} \end{array}\right] \begin{pmatrix} \mathbf{x} \\ -- \\ \hat{\mathbf{x}} \end{pmatrix} \tag{14}$$

For the decoupled-control analysis, $\mathbf{K}$ is replaced by $\mathbf{F}$ in equation (14) and the term

$$\left[\begin{array}{cc} \mathbf{B}_{18\times6} & \mathbf{G}_{6\times6} \\ \hline \mathbf{B}'_{12\times6} & \mathbf{G}_{6\times6} \end{array}\right] \mathbf{v}$$

is added to the right side of the equation. The subscripts indicate the dimensions of the various elements for the case in which the three residual modes are not estimated, which was used throughout the current analysis. With precalculated values for $\mathbf{K}'$ and $\mathbf{K}$ (or $\mathbf{K}'$, $\mathbf{F}$, and $\mathbf{G}$), the composite set of equations was integrated to obtain time-history responses for specified initial conditions in the various modes. In determining the estimator gain matrix, the weighting matrices $\mathbf{S}$ and $\mathbf{U}$ for the states and observations, which are analogous to the covariance intensities of $\mathbf{s}$ and $\mathbf{u}$, were varied until acceptable performance (satisfactory estimator eigenvalues and realistic gain values) was obtained. The resulting matrices were

$$\mathbf{S} = \text{diag}(.1,\ .1,\ .1,\ 10^5,\ 10^5,\ 10^5,\ .1,\ .1,\ ...,\ .1)$$

$$\mathbf{U} = \text{diag}(1,\ 1,\ 1,\ 1,\ 1,\ 1000)$$

The weighting value of 1000 gave the best results as far as control oscillations were concerned.

A block diagram for decoupled control is shown in sketch B. (A block diagram for LQR control is the same, with the exclusion of the $\mathbf{G}$ matrix.)

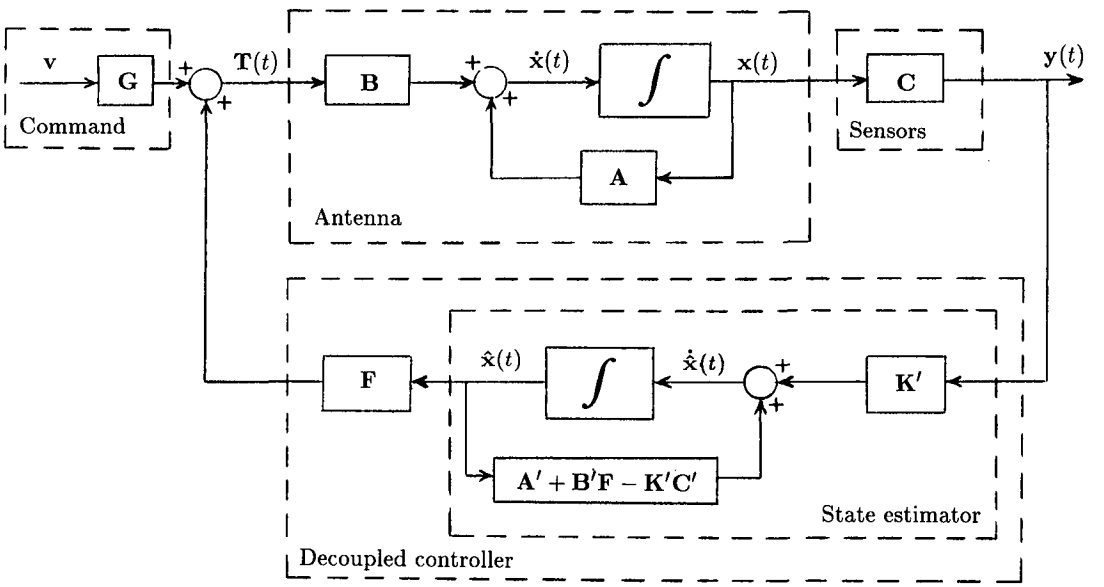

Sketch B

Method of Analysis

For the study, errors were incorporated in the individual sets of model parameters, one parameter at a time. For example, the effect of errors in knowledge of the flexible-mode natural frequencies ω_n was studied with the assumption that the values of all other model parameters were correct. Random sets of positive and negative errors were employed for investigating the effects of frequency and mode-slope error. (For example, see table III.) Effects of errors in damping and moment of inertia were investigated for either positive or negative errors. As previously described, the frequency errors are reflected in the plant matrix $\mathbf{A}$, which is a top element in equation (14). Errors in the damping ratio are also associated with the $\mathbf{A}$ matrix. Errors in the moments of inertia are associated with the $\mathbf{B}$ matrix, and for errors in the mode slopes, both the $\mathbf{B}$ and $\mathbf{C}$ matrices are affected. The feedback gain matrices $\mathbf{K}$ or $\mathbf{F}$, as well as the estimator gain matrix $\mathbf{K}'$, were computed using the nominal (no errors) $\mathbf{A}'$, $\mathbf{B}'$, and $\mathbf{C}'$ matrices. Also, these matrices were employed for the estimator in equation (14). The resulting eigenvalues for the composite set of equations (see eq. (14)) were checked for stability for each set of random errors used.

Results and Discussion

Results of the study are presented to illustrate effects of various model errors on the control system performance with regard to stability, time to null, and control requirements. The effects are analyzed either for (1) nulling initial disturbances in the rigid-body modes, or (2) nulling initial disturbances in the first three flexible modes. Case (1) is referred to as "rigid-body control," even though control is being applied to attempt to maintain the first three flexible modes at 0. Similarly, case (2) is referred to as "flexible-mode control." Comparisons are made between the decoupled and LQR control procedures with the results shown in tabular form, parametric plots, and as sample time histories of modal-amplitude and control responses. Comparisons are also made for the effects on the transients of the undisturbed modes.

Momentum and the maximum value for torque input are used as the measure of control requirements when making various comparisons. The momentum time histories represent the area under the torque response curves. The momentum values in the tables and parametric plots are the values at the end of each computer run, when the torque responses have essentially zeroed out. Maximum torque is the value for that actuator requiring the highest absolute value of torque.

General Considerations

For simulation, two three-axis CMG's were employed as actuators to control initial disturbances of 0.01 rad in the rigid-body modes or 1 in. in the three flexible mode amplitudes. Since the system equations are linear, the results can be scaled to any constant positive multiple of these initial conditions. Initial disturbances were also included in the three residual modes, even though it was determined that the results were not materially affected by their inclusion. (See ref. 4.) The CMG's were placed at the top and bottom of the antenna column at locations 1 and 2 as shown in figure 1. It was assumed that three-axis attitude sensors and three-axis attitude-rate sensors were available at various locations on the column for determining estimates of the state variables. Unless otherwise specified, one three-axis attitude-rate sensor at location 1 and one three-axis attitude sensor at location 4 were used.

It was further assumed that the control system was not activated until the initial state estimates were known to within 10 percent of true values for the rigid-body modes and for the first three flexible modes. The initial state estimates are actually the initial conditions in the estimator equations. Estimates of the residual modes were not included in the control procedure. Further discussion concerning initial estimates is given in the following section.

Effect of Model Error on Initial Estimates

As shown in reference 4, good estimates of the state variables are required before activating the control system, especially for rigid-body control. Without good estimates, the control requirements are excessive. Good estimates can be assured by running the estimator a few seconds before turning on the controller. The time histories of estimator error for rigid-body control are shown in figure 3. As expected, these time histories are unaffected by any type of model error up to the magnitudes considered in this study. The curves in figure 3 show that good estimates (90 percent) of the rigid-body disturbances are obtained within about 12 sec.

Figure 4 shows examples of the important effects of model errors in determining the state estimates for flexible-mode control before the controller is turned on. The effects can be compared to the case with no model errors, as shown in figure 4(a). Figure 4(b) shows that with $\mathbf{\Phi}'$ errors of ± 20 percent, state

estimation accuracy after about 6 sec is about 80 percent. It was determined that for Φ' errors of ± 50 percent, the state estimates attained only about 50 percent accuracy in 6 sec. Figures 4(c) and 4(d) indicate that ω_n errors are more crucial than Φ' errors with regard to the initial accuracy of the state estimates. For ω_n errors of ± 20 percent, the initial state estimates are shown to be good to only about 50 percent. For large ω_n errors (± 50 percent), the observer was marginally stable. Errors in the moments of inertia and damping ratios had practically no effect on the initial state estimates.

As previously stated, the results in this paper pertain to the assumption that the initial state estimates are within 10 percent of the true values at the time that the control is turned on. These results, however, are applicable to larger percentage errors in the estimates, inasmuch as reference 4 shows that satisfactory control performance for flexible-mode control is obtained for initial state estimates that were within 40 percent of the true values.

Effect of Model Frequency Error on Control Performance

Flexible-mode control. Figure 5 shows sample time histories of modal responses and control requirements for two sets of ω_n errors. For both control procedures, only small differences are noted in the flexible-mode responses between the two sets of errors. As shown in figure 5, the responses null within about 10 sec. The relatively small transients in the rigid-body responses are primarily caused by the observer in that perfect estimates of the state variables are not possible. (See ref. 4.) In addition, transients in the undisturbed modes (initially at 0) are inherent to the LQR control procedure. As shown, the rigid-body transient responses null in about 60 sec for both control procedures. Curves for no-error cases are not shown in figure 5 because they would fall within the general region of the plotted curves. For larger errors in ω_n, the effects are analyzed in a subsequent section of this paper.

The torque time histories in figure 5 require instantaneous values because the initial estimates were not 0. This condition can be eliminated by incorporating small time lags in the control-feedback gain matrix. (See ref. 4.) It is of interest to note in figure 5(a) that the control actuator requiring the maximum absolute value of torque is different for the positive- and negative-error cases. This design consideration is important in sizing the actuators. Figure 5 shows that for LQR control, the total momentum for the six actuators is somewhat lower for the case with an ω_n error of -10 percent.

The parametric plots in figure 6 show the changes in the flexible-mode control requirements from their nominal (no-error) values over a range of ω_n errors of specified magnitudes. The sets for determining the random errors used in the frequency-error analysis are shown in table III. The eight sets represent the total number of combinations possible for the first three flexible modes. As shown, random errors were also incorporated in the three residual modes, although it was determined that their effects were relatively small. The eight sets of random signs shown in table III were used to generate constant percentage errors in the six flexible-mode frequencies at specific magnitudes of frequency error ranging from 10 to 50 percent. (It should be noted that in figure 6, data for all eight sets of random errors are not shown at each specific magnitude of error because some points coincide.) The system was stable over the range of ω_n errors shown, but instability occurred for ω_n errors of ± 75 percent. As shown, the effect on total momentum is larger for decoupled control for ω_n errors of more than 20 percent; the effect on maximum torque is larger for LQR control over the entire range of ω_n error. For both control procedures, it should be noted that the z-axis control actuator at location 1 (fig. 1) required the maximum torque in the nominal case. In some decoupled cases with an ω_n error, the z-axis actuator at location 2 required the maximum torque. For the LQR cases represented by the two lowest data points across the range of ω_n errors, the y-axis actuator at location 1 required the maximum torque.

Rigid-body control. The parametric plots in figures 7 and 8 show the effects of ω_n errors on rigid-body control requirements. As expected, the changes in the control requirements are considerably smaller for rigid-body control than for flexible-mode control. In figure 7, only the maximum positive and negative changes in torque are plotted for the eight cases (table III) at each magnitude of ω_n error. From the figure, it is evident that effects on maximum torque are essentially the same for both control procedures. In all cases, the x-axis control actuator at location 2 required the maximum torque. As for total momentum requirements, figure 8 shows that ω_n errors have a negligible effect for decoupled control.

In reference 4 it was shown that the rigid-body modes could be controlled adequately with the use of only one three-axis attitude sensor at location 1. Hence, an error analysis was made for this condition (i.e., no rate sensor). The results are presented in table IV for seven sets of random errors in ω_n ranging from 10 to 20 percent. (No figure is presented because variations were relatively small.) The data

indicate that an unstable control system can result with an ω_n error greater than 10 percent. For example, with an ω_n error of 15 percent, the ψ rigid-body mode became unstable for LQR control. For an ω_n error of 20 percent, the same mode was unstable along with one of the first three flexible modes. For the stable cases, it is seen that the maximum torque is unaffected. Also, in two of the cases for LQR control with an ω_n error of 10 percent, the effects on momentum were relatively large as a result of poor performance by the z-axis actuators. This performance is characterized by the long control oscillations that require more than 60 sec to zero out, as shown in figure 9. Also shown in figure 9 is an example of poor response in the ψ rigid-body mode and a relatively large transient response for the first flexible mode. The ϕ and θ rigid-body mode responses are not affected.

Figure 10(a) shows an example of the effect of observation spillover (effect of residual modes) on the z-axis control actuator at location 1 for decoupled control. The other actuators are essentially unaffected. The rapid control oscillations, although small in magnitude, are inherent to the decoupled-control procedure, with or without model error, and are aggravated by the effect of model error. These oscillations are eliminated if estimates of the residual modes can be included in the control procedure. (See ref. 4.) An alternative would be to turn off the actuator, as shown in figure 10(b). (This condition was simulated on the computer by zeroing out the third row in the feedback gain matrix. The other gains in the matrix were left unchanged, with the result that the control law was not altered.) The system remained stable with only minor effects noticed for the first and third flexible modes.

Effect of Model Damping Error on Control Performance

The results in table V show that model damping error has little effect on the control requirements, regardless of whether the error is positive or negative. The effect is greater for flexible-mode control; however, the larger changes are shown to be negative, a result that is not detrimental. (The maximum negative error of 50 percent was chosen because some natural damping is required for stability.)

As expected, a negative ζ_n error has a detrimental effect on control actuator performance because of an increase in the observation spillover effect caused by the reduced damping. The time histories in figure 11 depict this effect on the performance of the z-axis control actuator at location 2. (The other actuators are not affected.) Rapid control oscillations for both decoupled and LQR flexible-mode control are shown in figures 11(a) and 11(b). The LQR oscillations in figure 11(b) are more pronounced; however, after about 6 sec, their magnitudes are about the same as those for decoupled control. (The oscillations can be partially alleviated if estimates of the residual modes can be included in the control procedure.) Figure 11(c) is based on the case for figure 11(b) except that the damping error is limited to the first three flexible modes. This situation is not likely to occur, but the fact that the oscillations are smaller than those in figure 11(b) points out the adverse effect of negative ζ_n error on control performance. The effect of positive ζ_n error is not as great, as is seen in figure 11(d) for LQR control. Decoupled control was not affected.

Effect of Model Moment-of-Inertia Error on Control Performance

Figure 12 summarizes the effect of model moment-of-inertia error on the momentum requirements for rigid-body and flexible-mode control. Maximum torque requirements are not materially affected. As shown, changes in momentum are relatively small over the large range of positive and negative errors in inertia, especially for flexible-mode control. Note that in this case, the effect of LQR control is three times larger than for decoupled control.

Effect of Mode-Slope Error on Control Performance

Consideration of the 15 different nonzero mode slopes included in the **B** and **C** matrices would yield 32 768 (i.e., 2^{15}) possible combinations of random sets of positive and negative errors for any specified magnitude of $\mathbf{\Phi}'$ error. Twenty random sets of errors (similar to those given in table III) at four values of $\mathbf{\Phi}'$ error were selected to determine the maximum changes in control requirements, as shown in figure 13. Each random set was selected to be radically different from other sets because it was found that a change of one or two signs between any two sets had a negligible effect on the results; thus each set essentially represents 120 or more different sets. This value was derived by the following combinatorial formula for the number of r elements out of a set of n for a total of 120 combinations.

$$\mathbf{C}_r^n = \frac{n(n-1)\cdots(n-r+1)}{1\cdot 2\cdots r}$$

where

$$\mathbf{C}_1^{15} = \frac{15}{1} = 15$$

and

$$\mathbf{C}_2^{15} = \frac{15\cdot 14}{1\cdot 2} = 105$$

The 20 random sets chosen for the current analysis are deemed adequate for establishing the maximum effects. The system was stable over the range of $\mathbf{\Phi}'$ errors shown. Although errors of ± 75 percent resulted in a stable system, the control requirements were excessive for flexible-mode control. (For example, momentum changes exceeded 300 percent.)

As expected, the results in figure 13 show only small effects of $\mathbf{\Phi}'$ errors on the rigid-body requirements. It is evident that when controlling the flexible modes, the maximum torque is more sensitive to $\mathbf{\Phi}'$ error for decoupled control than for LQR control. In all cases resulting in increased torque for LQR rigid-body and flexible-mode control, the control actuator requiring the maximum value was the same as that for the nominal case. For the decoupled flexible-mode control cases resulting in the largest torque increases, the z-axis actuator at location 2 required the maximum torque.

Comparison of the results in figure 13 with those in figures 6 and 8 shows that the maximum changes in momentum are comparable for $\mathbf{\Phi}'$ and ω_n errors. The larger errors in $\mathbf{\Phi}'$ are considered to be more realistic because mode shapes and slopes are the least identifiable of the model parameters and are therefore the most important of all the model errors. (See ref. 8.) Hence, it would be advisable to concentrate on $\mathbf{\Phi}'$ in any initial adaptive control procedure when updating the model parameters.

Effect of Model Error on Maximum Transients

As previously discussed, transients are produced in the undisturbed modes when either control procedure is employed, but transients are more pronounced with LQR control. Model errors in ω_n and $\mathbf{\Phi}'$ affect the maximum values of these transients, as summarized in table VI. The last column indicates the importance of the particular effect for each control procedure. (For example, a small effect represents a relatively small change in the transients over a large range in model error.) The example in figure 14 illustrates the large effect on the flexible mode transients due to an ω_n error using LQR rigid-body control. It is seen in table VI(a) that this effect increases substantially as the ω_n error increases. (Errors in ς_n and in inertia have negligible effects on the rigid-body and flexible-mode transients.)

Figure 15 illustrates a serious effect of ω_n and $\mathbf{\Phi}'$ errors on the ψ rigid-body transient response during flexible-mode control for both control procedures. Although the maximum transients are only about $0.2°$, it is apparent that a considerable period of time is required before the ψ responses null. (The other two rigid-body responses, θ and ϕ, null in 60 sec.) For smaller errors in ω_n and $\mathbf{\Phi}'$, say 25 percent, the ψ transient nulls within 60 to 120 sec.

Effect of Model Error on Time to Null

Examples of the effect of various model errors on the time to null are presented in figures 16 and 17. Figure 16(a) shows that for large ω_n errors with decoupled flexible-mode control, the time to null is about 60 sec. For the more realistic errors in figure 16(c), this time is reduced considerably. The results shown in figures 16(e) and 16(f) for large $\mathbf{\Phi}'$ errors are similar to those shown in figure 16(a). With a few exceptions, model error had no effect on time to null for rigid-body control for either control procedure. Some LQR cases with ω_n errors larger than 20 percent required up to 150 sec to null the ψ response as well as the first flexible-mode transient. There is also some effect of model inertia error I on time to null, as illustrated in figure 17. (Note the expanded time scale.) The curves apply to both control procedures.

Concluding Remarks

An analysis has been made to determine the effects of model error on the control of a large flexible space antenna. Control was achieved by employing two three-axis control-moment gyros (CMG's) located on the antenna column. Results have been compared for decoupled and linear quadratic regulator (LQR) control procedures. Errors were assumed to exist in the individual model parameters: modal frequency, modal damping, mode slope, and moment of inertia. Their effects on control-system performance have been analyzed either for (1) nulling initial disturbances in the rigid-body modes, or (2) nulling initial disturbances in the first three flexible modes. The study includes the effects on stability, time to null, and control requirements (defined as maximum torque and total momentum), as well as on the accuracy of obtaining initial state estimates before the controller is activated. The effects on the transients of the undisturbed modes (initially at 0) have also been included.

Errors in the model natural frequencies ω_n have the largest effect on the accuracy of determining initial estimates for the state variables. Model errors in the mode slopes have the next largest effect; errors in the damping and moment-of-inertia parameters have a negligible effect. For the wide range of model errors investigated, only large errors in frequency (> 50 percent) resulted in an unstable system.

Effects of model errors on the control requirements (defined as maximum torque and total

momentum) are, in general, comparable for both control procedures. The effect of mode-slope error appears to be the largest of all model errors. Hence, it would be advisable to concentrate on this parameter in any initial adaptive control procedure when updating the model parameters. Errors in the damping and moment-of-inertia parameters have only small effects on the control requirements. However, negative damping error is detrimental to control-actuator performance in that rapid oscillations are induced in the control responses.

In some cases for flexible-mode control with frequency or mode-slope errors, the control actuator requiring the maximum absolute value of torque is different from the nominal (no-error) case. This difference would be an important design consideration when sizing the actuators.

The effects of model errors in frequency and mode slope on the maximum transients of the undisturbed modes are different for the two control procedures, the severity depending upon the type of model error and whether rigid-body modes or flexible modes are to be controlled. The largest effect is produced by frequency errors with rigid-body LQR control. Model errors in the damping and moment-of-inertia parameters have a negligible effect on the transients.

For rigid-body control, the model errors have only a minor effect on the time to null. Although the effect is larger for flexible-mode control, the responses nulled within 60 sec in all cases.

NASA Langley Research Center
Hampton, VA 23665-5225
May 27, 1986

Appendix

Tables of Matrices Used in Current Analysis

This appendix consists of tables of matrices (tables AI to AIV) used in the current analysis for the **B** matrix, **F** matrix for decoupled control, **K** matrix and **Q** weightings for LQR control, and the **C** matrix.

TABLE AI. **B** MATRIX

$\mathbf{B}_{18\times 6}$

0.	0.	0.	0.	0.	0.
0.	0.	0.	0.	0.	0.
0.	0.	0.	0.	0.	0.
0.	0.	0.	0.	0.	0.
0.	0.	0.	0.	0.	0.
0.	0.	0.	0.	0.	0.
0.	0.	0.	0.	0.	0.
0.	0.	0.	0.	0.	0.
0.	0.	0.	0.	0.	0.
.19737917E-07	0.	.11003987E-09	.19737917E-07	0.	.11003987E-09
0.	.19658120E-07	0.	0.	.19658120E-07	0.
.11003987E-09	0.	.25777798E-07	.11003987E-09	0.	.25777798E-07
.14712325E-05	0.	-.11745441E-03	-.42320542E-06	0.	-.37776195E-06
0.	-.36681003E-03	0.	0.	.31838614E-04	0.
.61143590E-03	0.	.89756447E-04	-.61885513F-04	0.	.20098311E-05
-.39176798E-06	0.	.44199044E-05	.88746034F-07	0.	-.10276237E-03
-.12698521E-03	0.	-.11452151E-04	-.21981567E-02	0.	-.83552937E-06
.59589099E-07	0.	-.34274029E-05	.71689636E-07	0.	-.13551496E-03

TABLE AII. **F** MATRIX USED FOR DECOUPLED CONTROL

$\mathbf{F}_{6\times 12}$

Row no. 1	-.46716861E+05	0.	.11921819E+04	0.	0.	0.
	-.84090349E+06	0.	.21459275E+05	-.96181672E+03	0.	-.11606566E+04
2	0.	-.40617932E+05	0.	0.	0.	0.
	0.	-.73112277E+06	0.	0.	.22278945E+04	0.
3	.10686118E+04	0.	.12631355E+04	0.	0.	0.
	.19235012E+05	0.	.22736439E+05	.73813685E+04	0.	-.18777995E+02
4	-.45993428E+06	0.	.97060274E+03	0.	0.	0.
	-.82788170E+07	0.	.17470849E+05	.96181672E+03	0.	.11606566E+04
5	0.	-.46807772E+06	0.	0.	0.	0.
	0.	-.84253990E+07	0.	0.	-.22278945E+04	0.
6	.10941729E+04	0.	-.38920310E+06	0.	0.	0.
	.19695112E+05	0.	-.70056557E+07	-.73813685E+04	0.	.18777995E+02

TABLE AIII. **K** MATRIX and **Q** WEIGHTINGS USED FOR LQR CONTROL

$K_{6\times12}$

Row no. 1	-.298954E+06	0.	.549278E+04	-.164308E+03	0.	-.217185E+03	-.496916E+07	0.
	.105906E+06	-.379852E+03	0.	-.265962E+04				
2	0.	-.293977E+06	0.	0.	.298704E+03	0.	0.	-.493832E+07
	0.	0.	.363859E+04	0.				
3	-.643776E+04	0.	-.165435E+06	.446188E+03	0.	-.160382E+03	-.111494E+06	0.
	-.327119E+07	.619151E+04	0.	-.324594E+03				
4	-.332541E+06	0.	-.921316E+03	.915410E+00	0.	-.234356E+03	-.535499E+07	0.
	-.134411E+05	.804148E+02	0.	.281736E+03				
5	0.	-.337012E+06	0.	0.	.319770E+03	0.	0.	-.543606E+07
	0.	0.	-.342500E+03	0.				
6	-.128526E+04	0.	-.205592E+06	.519965E+03	0.	-.221741E+02	-.124421E+05	0.
	-.380137E+07	-.935697E+02	0.	-.362612E+01				

$Q = \text{diag}(0.2 \times 10^{12}, 0.2 \times 10^{12}, 0.7 \times 10^{11}, 1, 1, 1, 0.2 \times 10^{14}, 0.2 \times 10^{14}, 0.92 \times 10^{13}, 0.41 \times 10^{8}, 0.14 \times 10^{8}, 0.76 \times 10^{7})$

TABLE AIV. **C** MATRIX FOR THREE-AXIS ATTITUDE-RATE SENSOR AT LOCATION 1 AND THREE-AXIS ATTITUDE SENSOR AT LOCATION 4

$C_{6\times18}$

Row no. 1	0.	0.	0.	0.	0.	0.
	0.	0.	0.	.10000000E+01	0.	0.
	.22532850E-03	0.	.18790460E-02	-.11935500E-06	-.25308020E-03	.43113600E-04
2	0.	0.	0.	0.	0.	0.
	0.	0.	0.	0.	.10000000E+01	0.
	0.	-.19195410E-02	0.	0.	0.	0.
3	0.	0.	0.	0.	0.	0.
	0.	0.	0.	0.	0.	.10000000E+01
	-.17988610E-01	0.	.27583180E-03	.13464720E-05	-.22823800E-04	-.24797850E-02
4	.10000000E+01	0.	0.	-.11818080E-03	0.	-.50625030E-03
	.23921470E-07	.30756450E-03	-.43030160E-05	0.	0.	0.
	0.	0.	0.	0.	0.	0.
5	0.	.10000000E+01	0.	0.	.54079040E-03	0.
	0.	0.	0.	0.	0.	0.
	0.	0.	0.	0.	0.	0.
6	0.	0.	.10000000E+01	-.10959970E-01	0.	.17061950E-03
	.37009500E-04	-.14806800E-04	-.24551710E-01	0.	0.	0.
	0.	0.	0.	0.	0.	0.

References

1. Sundararajan, N.; and Montgomery, Raymond C.: Progress in Adaptive Control of Flexible Spacecraft Using Lattice Filters. Paper presented at Workshop on Applications of Adaptive Control (New Haven, Connecticut), Yale Univ., May 1985.
2. Sullivan, Marvin R.: *LSST (Hoop/Column) Maypole Antenna Development Program.* NASA CR-3558, Part 2, 1982.
3. Young, John W.; Hamer, Harold A.; and Johnson, Katherine G.: *Decoupled-Control Analysis of a Large Flexible Space Antenna With Linear Quadratic Regulator Comparisons.* NASA TP-2293, 1984.
4. Hamer, Harold A.; Johnson, Katherine G.; and Young, John W.: *Decoupled and Linear Quadratic Regulator Control of a Large, Flexible Space Antenna With an Observer in the Loop.* NASA TP-2484, 1985.
5. Joshi, Suresh M.: Control Systems Synthesis for a Large Flexible Space Antenna. *Acta Astronaut.*, vol. 10, no. 5-6, May-June 1983, pp. 365–380.
6. Kwakernaak, Huibert; and Sivan, Raphael: *Linear Optimal Control Systems.* John Wiley & Sons, Inc., c.1972.
7. Armstrong, Ernest S.: *ORACLS—A System for Linear-Quadratic-Gaussian Control Law Design.* NASA TP-1106, 1978.
8. Joshi, Suresh M.: Controller Design and Parameter Identifiability Studies for a Space Antenna. *Trans. Canadian Soc. Mech. Eng.*, vol. 9, no. 3, 1985, pp. 125–130.

TABLE I. ANTENNA CHARACTERISTICS

$$\begin{bmatrix} I_x = 1.9577 \times 10^{10} \text{ lb-in}^2;\ I_y = 1.9657 \times 10^{10} \text{ lb-in}^2; \\ I_z = 1.499 \times 10^{10} \text{ lb-in}^2;\ I_{xz} = 0.8357 \times 10^{8} \text{ lb-in}^2; \\ w = 10\,020.3 \text{ lb} \end{bmatrix}$$

Mode	ω_n, rad/sec	T_n, sec	ς_n	Description
1	0.7466	8.42	0.01	First torsion
2	1.3460	4.67	.01	First bending, xz-plane
3	1.7025	3.69	.01	First bending, yz-plane
4	3.1813	1.98	.01	Surface torsion
5	4.5294	1.39	.02	Second column bending, yz-plane
6	5.5905	1.12	.02	Surface-hoop torsion, feed-mast torsion

TABLE II. SPECIFIED CLOSED-LOOP EIGENVALUES

Case	Mode	ω_d, rad/sec	ς_d
Decoupled	θ	0.1	0.9
	ϕ	.1	.9
	ψ	.1	.9
	1	[a].7466	.59
	2	[a]1.346	.34
	3	[a]1.7025	.24
LQR	θ	0.098	0.904
	ϕ	.112	.900
	ψ	.112	.901
	1	.7453	.502
	2	1.345	.511
	3	1.700	.502

[a]Values used are exact ω_n values.

TABLE III. RANDOM SETS FOR ω_n ERRORS

Flexible mode	ω_n, rad/sec	Positive and negative errors for random set number—							
		1	2	3	4	5	6	7	8
1	0.7466	+	+	+	+	−	−	−	−
2	1.3460	+	+	−	−	−	−	+	+
3	1.7025	+	−	−	+	−	+	+	−
4	3.1813	+	−	+	−	−	−	−	−
5	4.5294	+	−	+	−	−	−	−	+
6	5.5905	+	−	−	−	−	−	−	+

TABLE IV. EFFECT OF ω_n ERRORS ON RIGID-BODY CONTROL REQUIREMENTS

[One three-axis attitude sensor]

Random error in ω_n, percent	$100(T_\epsilon - T_N)/T_N$, percent (*a*)		$100(M_\epsilon - M_N)/M_N$, percent (*a*)		Comments
	Decoupled (*b*)	LQR (*c*)	Decoupled (*b*)	LQR (*c*)	
±10	0	0	1.7	−1.4	
±10	0	0	−0.6	10.9	Long oscillations in $T_{z,1}$ and $T_{z,2}$ for LQR control
±10	0	0	1.9	−4.4	
±10	0	0	−0.7	17.7	Same as above
±15	0	0	−0.7	26.3	Same as above
±15	0	U	17.4	U	Long oscillations in $T_{z,1}$ and $T_{z,2}$ for decoupled control
±20	U	U	U	U	

[a]U indicates instability; 0 indicates negligible effect.
[b]For decoupled control: $T_N = 418$ ft-lb; $M_N = 10\,984$ ft-lb-sec.
[c]For LQR control: $T_N = 301$ ft-lb; $M_N = 11\,720$ ft-lb-sec.

TABLE V. EFFECT OF ς_n ERRORS ON CONTROL REQUIREMENTS

Condition	Error in ς_n, percent	$100(T_\epsilon - T_N)/T_N$, percent (a)		$100(M_\epsilon - M_N)/M_N$, percent (a)	
		Decoupled	LQR	Decoupled	LQR
Rigid-body control (one three-axis attitude sensor)	+900	0	0.3	0	−0.3
	−50	0	0	.1	.1
Rigid-body control (two three-axis sensors)	+900	−0.7	0.7	0	−0.2
	−50	0	0	.2	0
Flexible-mode control (two three-axis sensors)	+900	−9.5	−14.5	−5.4	−9.7
	−50	.4	1.8	3.7	4.0

[a]Values for T_N and M_N are given in figures 6 to 8 and in table IV; 0 indicates negligible effect.

TABLE VI. TYPICAL EFFECTS OF MODEL ERROR ON TRANSIENTS

(a) Rigid-body control

Model error in—	Error, percent	Control procedure	Maximum transients (absolute)			Effect
			A_1, in.	A_2, in.	A_3, in.	
ω_n	±10	Decoupled	0.003	0.014	0.022	Small
	±50		.005	.040	.027	
	±10	LQR	0.21	0.74	0.86	Large
	±50		.12	2.17	2.55	
$\mathbf{\Phi}'$	±10	Decoupled	0.002	0.035	0.020	Large
	±50		.005	.135	.175	
	±10	LQR	0.24	0.65	0.75	Small
	±50		.21	.80	.95	

(b) Flexible-mode control

Model error in—	Error, percent	Control procedure	Maximum transients (absolute)			Effect
			θ, rad	ϕ, rad	ψ, rad	
ω_n	±10	Decoupled	0.000013	0.000038	0.000405	Large
	±50		.000115	.000137	.003180	
	±10	LQR	0.000161	0.000233	0.001120	Small
	±50		.000194	.000349	.001440	
$\mathbf{\Phi}'$	±10	Decoupled	0.000033	0.000009	0.001040	Large
	±50		.000212	.000146	.003200	
	±10	LQR	0.000116	0.000270	0.001540	Small
	±50		.000078	.000080	.003960	

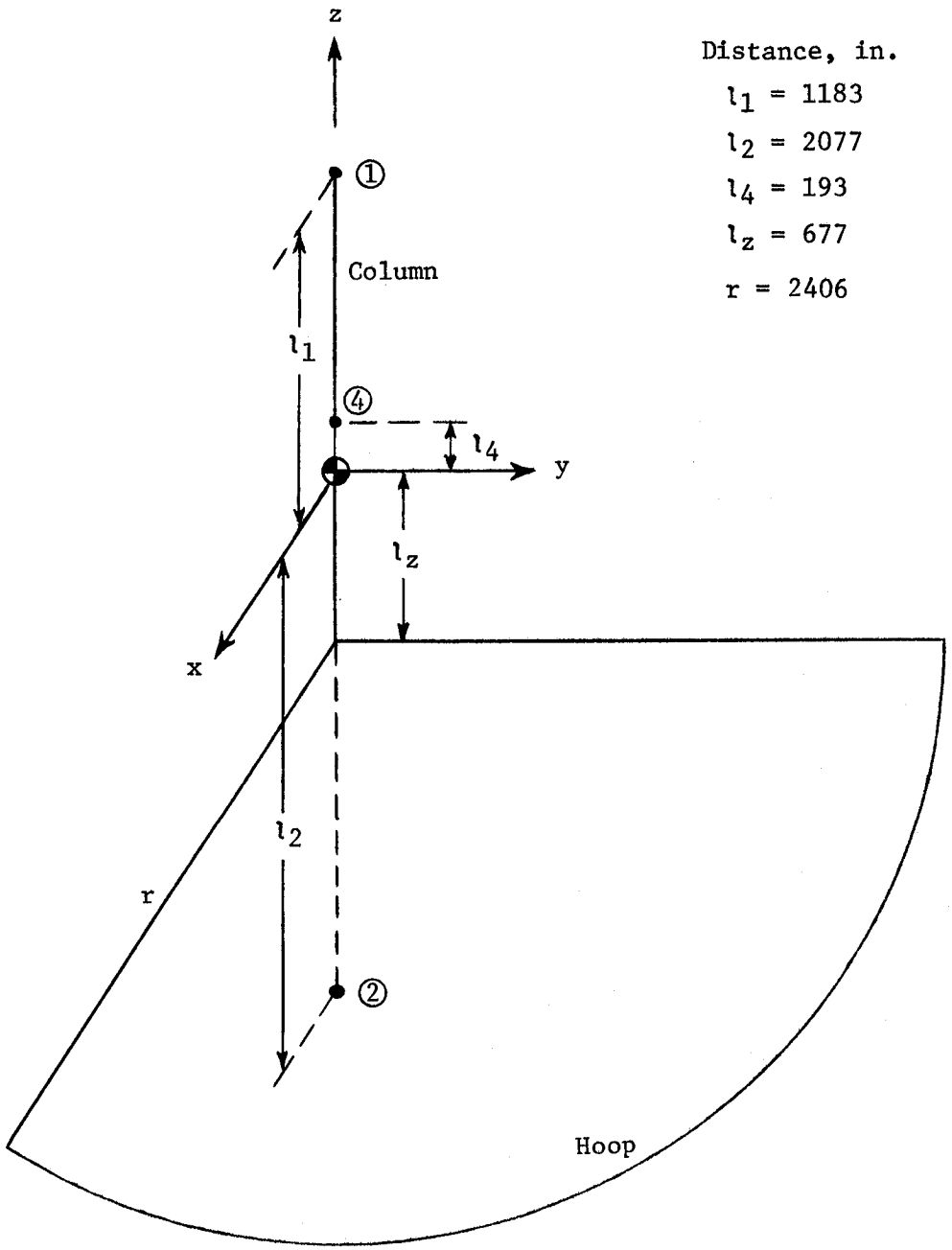

Figure 1. Antenna coordinates and actuator or sensor locations.

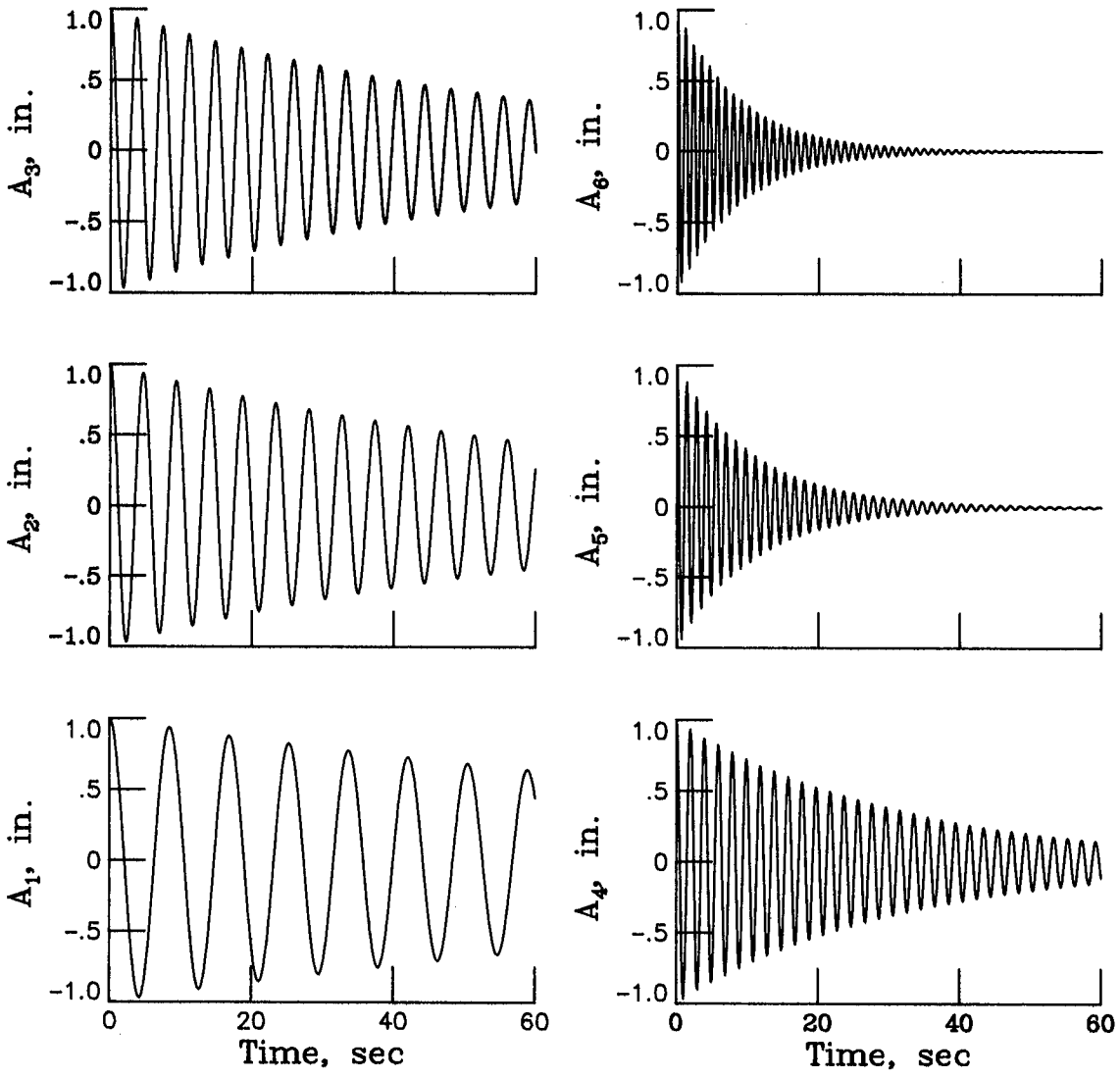

Figure 2. Unforced responses of natural vibration modes.

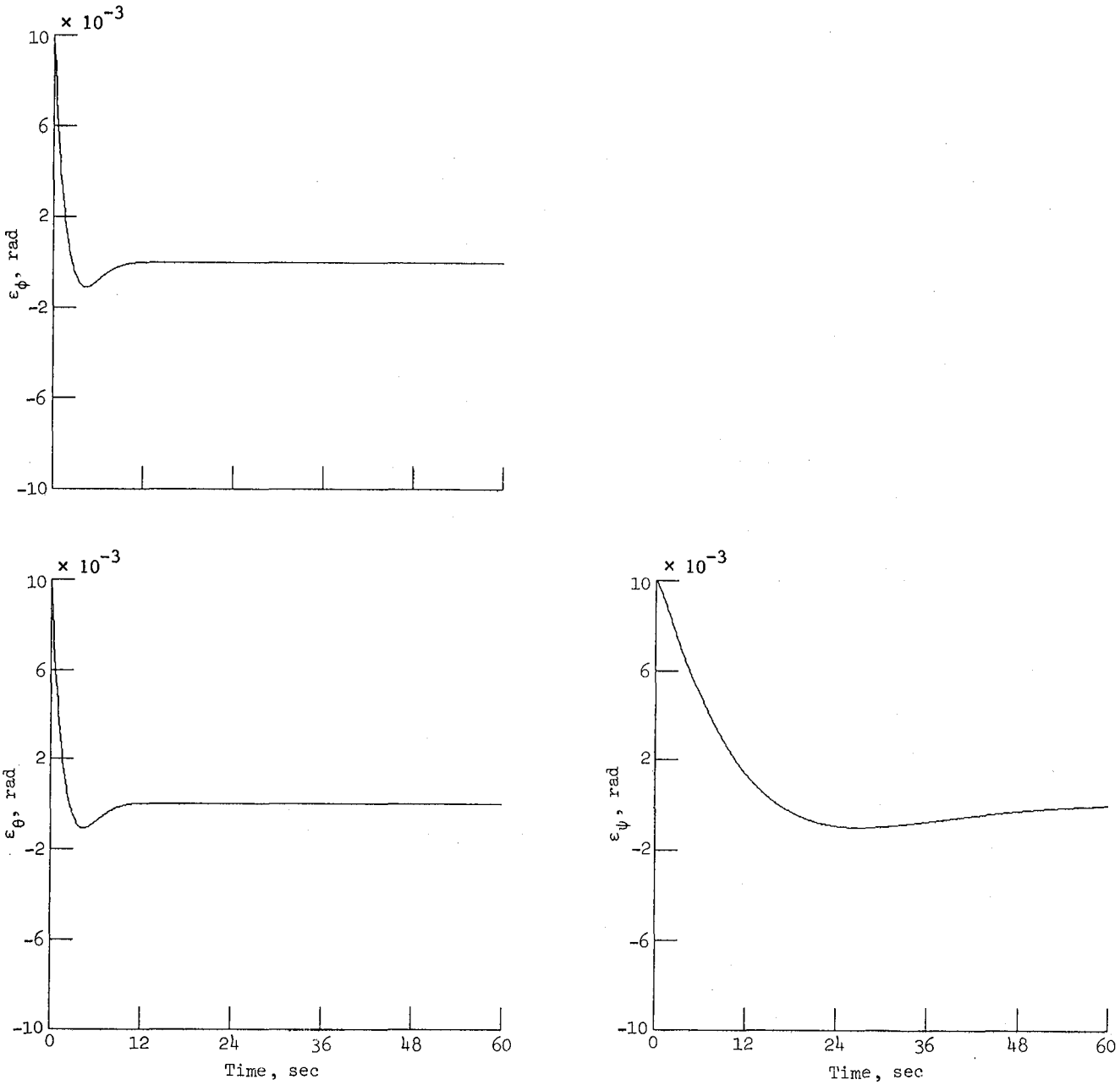

Figure 3. State estimation error for rigid-body control. Controls off.

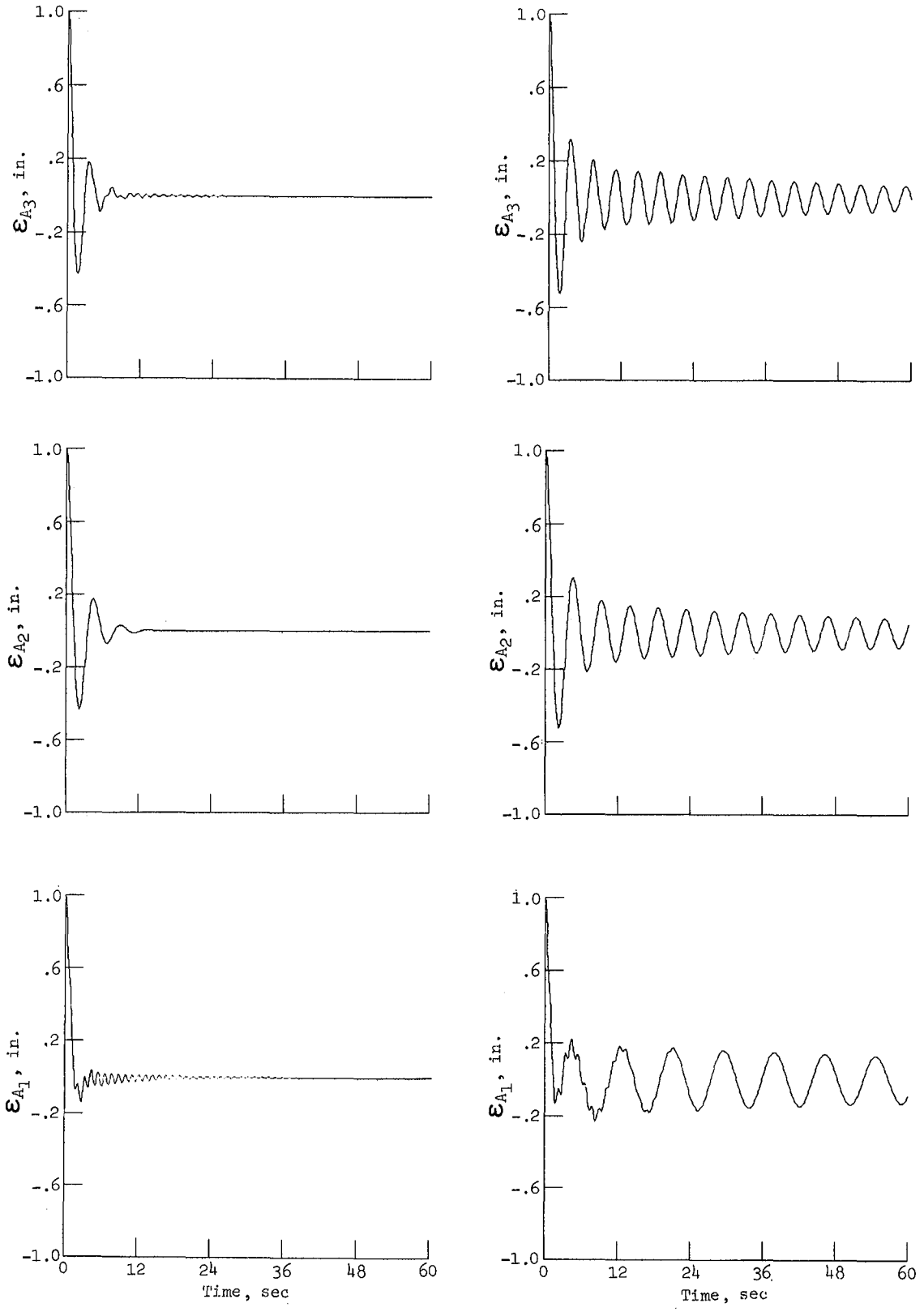

(a) No model errors.

(b) Error in Φ', ±20 percent.

Figure 4. Examples of state estimation error for flexible-mode control. Controls off.

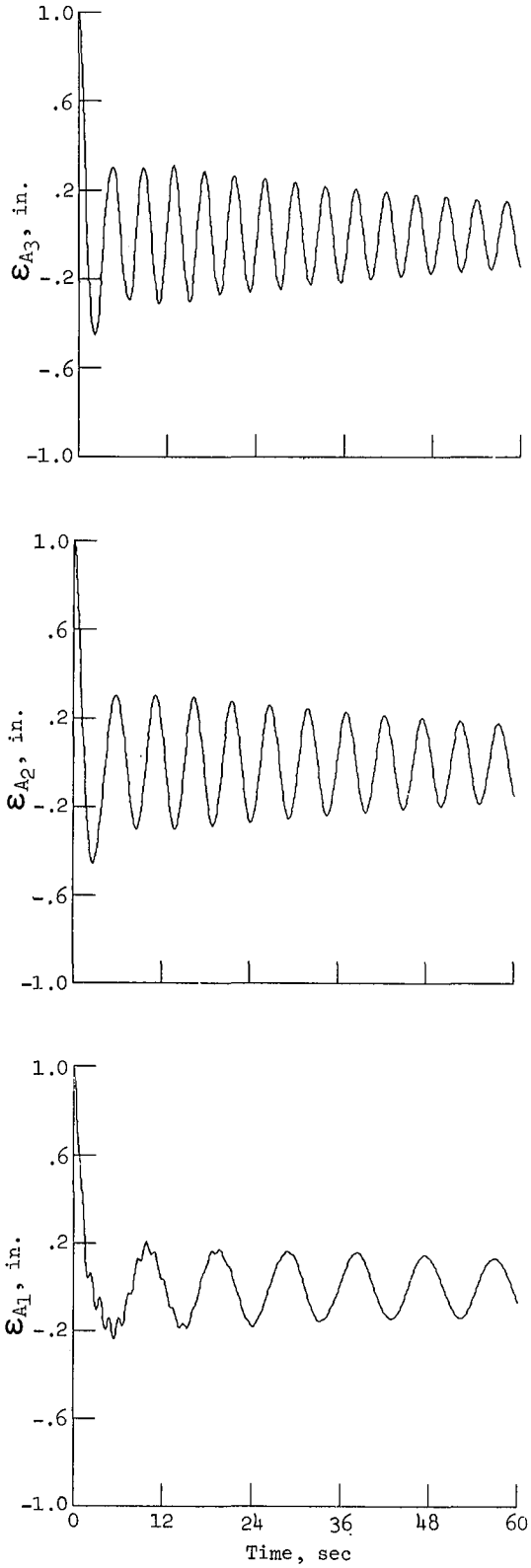

(c) Error in ω_n, ±10 percent.

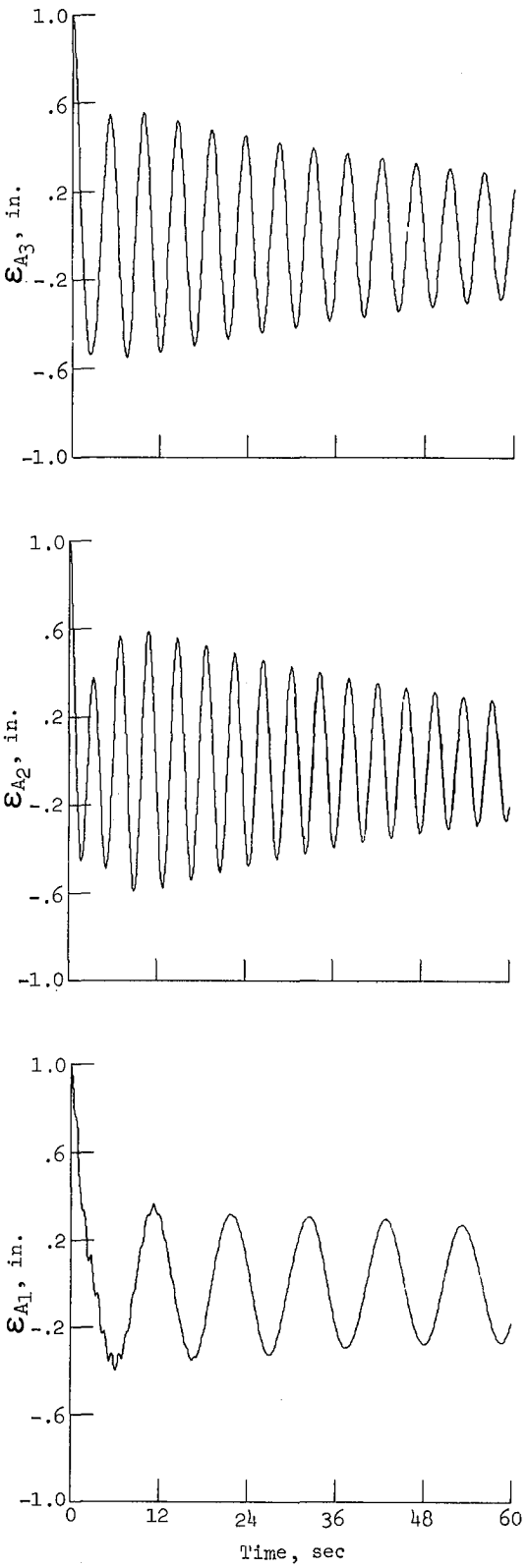

(d) Error in ω_n, ±20 percent.

Figure 4. Concluded.

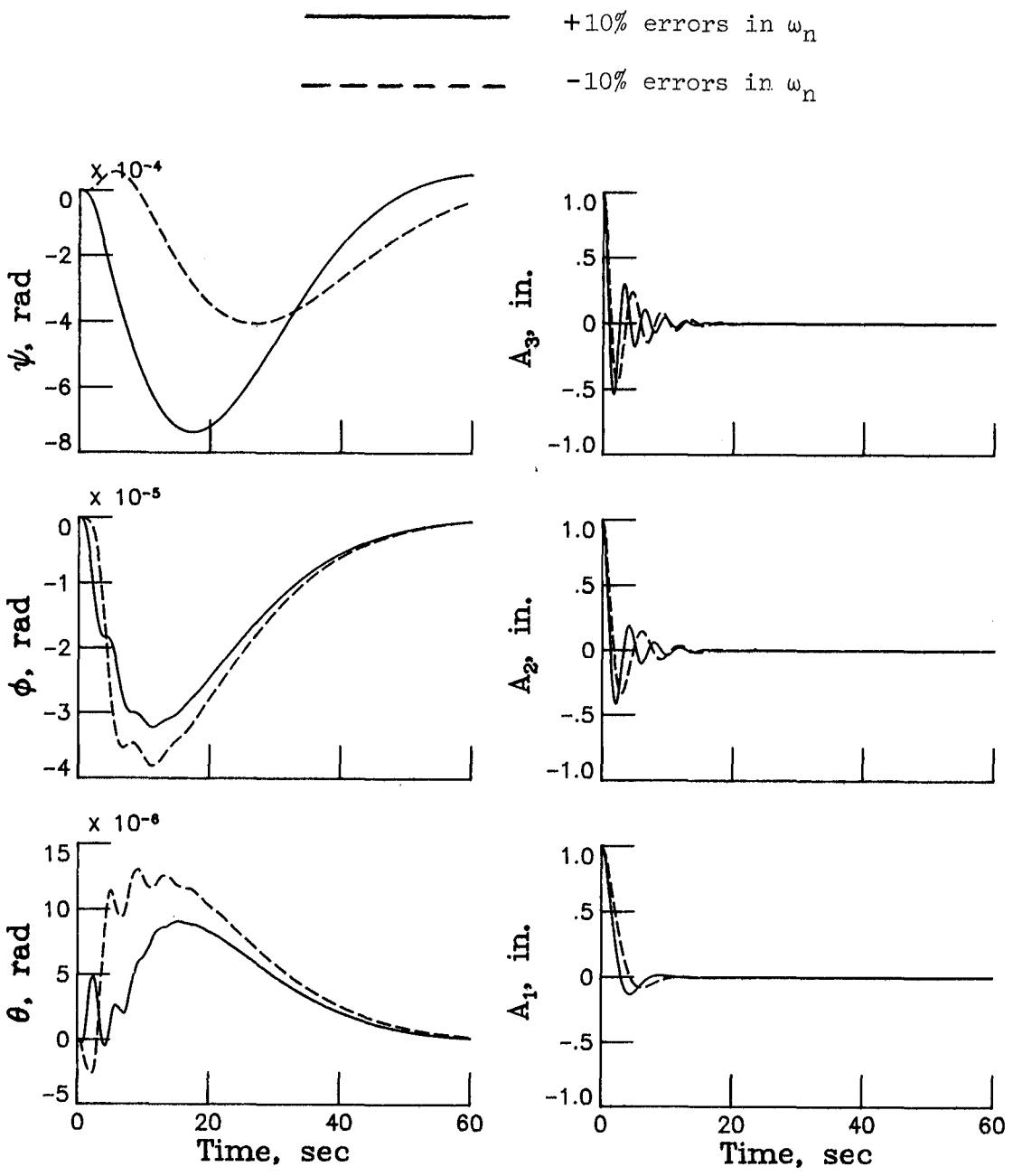

(a) Decoupled flexible-mode control.

Figure 5. Comparison of modal responses and control requirements for two sets of model frequency errors.

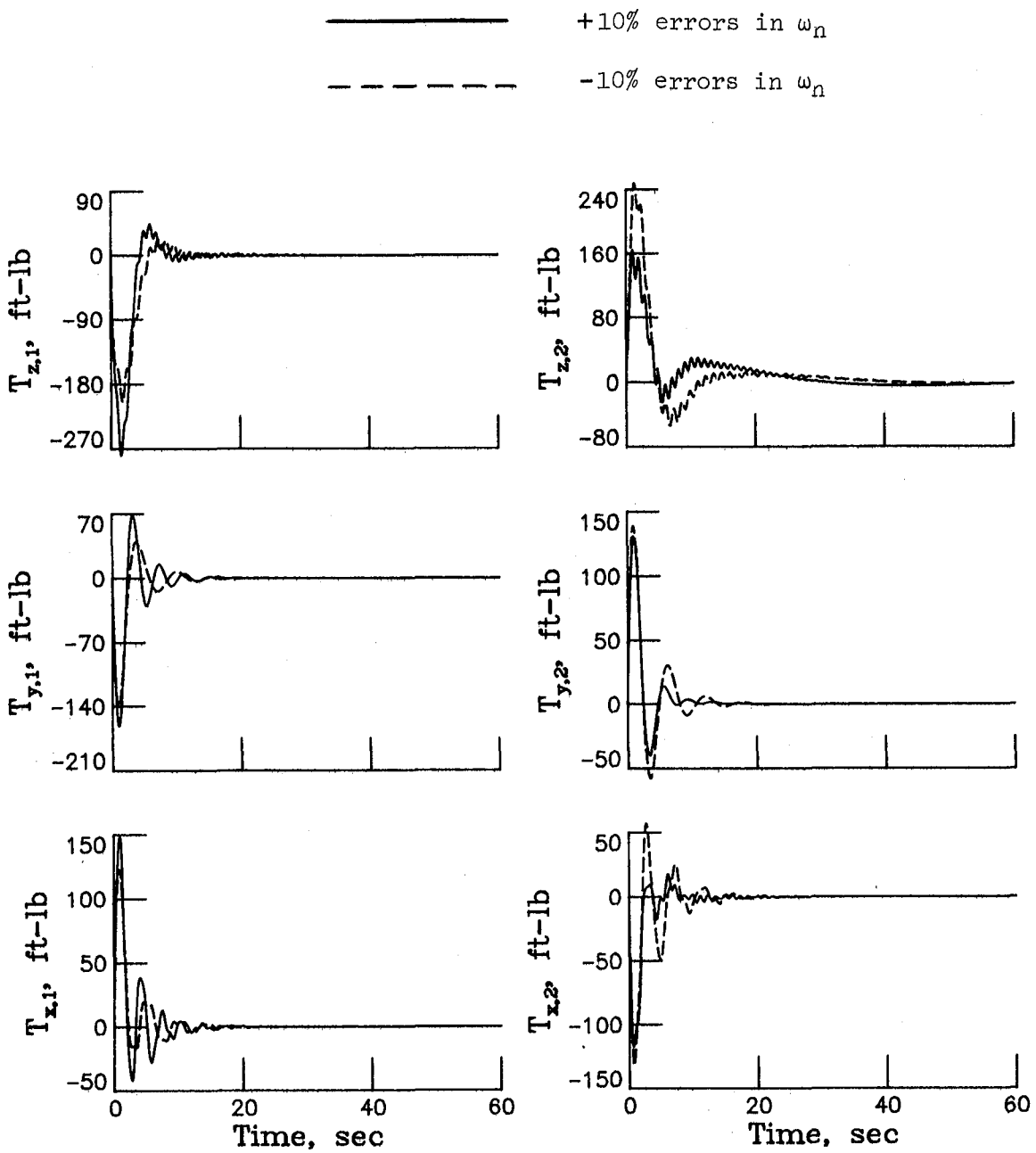

(a) Continued.

Figure 5. Continued.

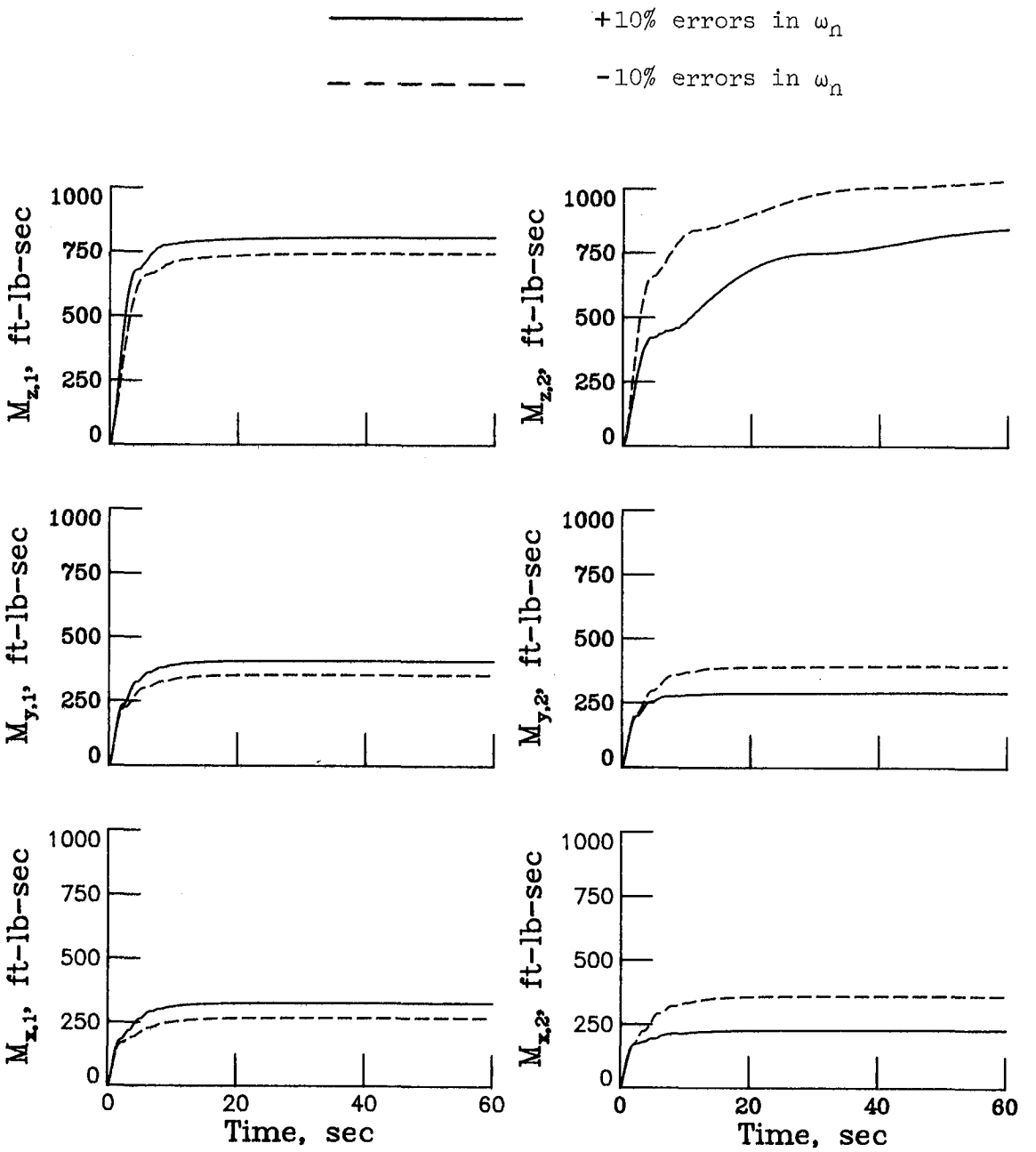

(a) Concluded.

Figure 5. Continued.

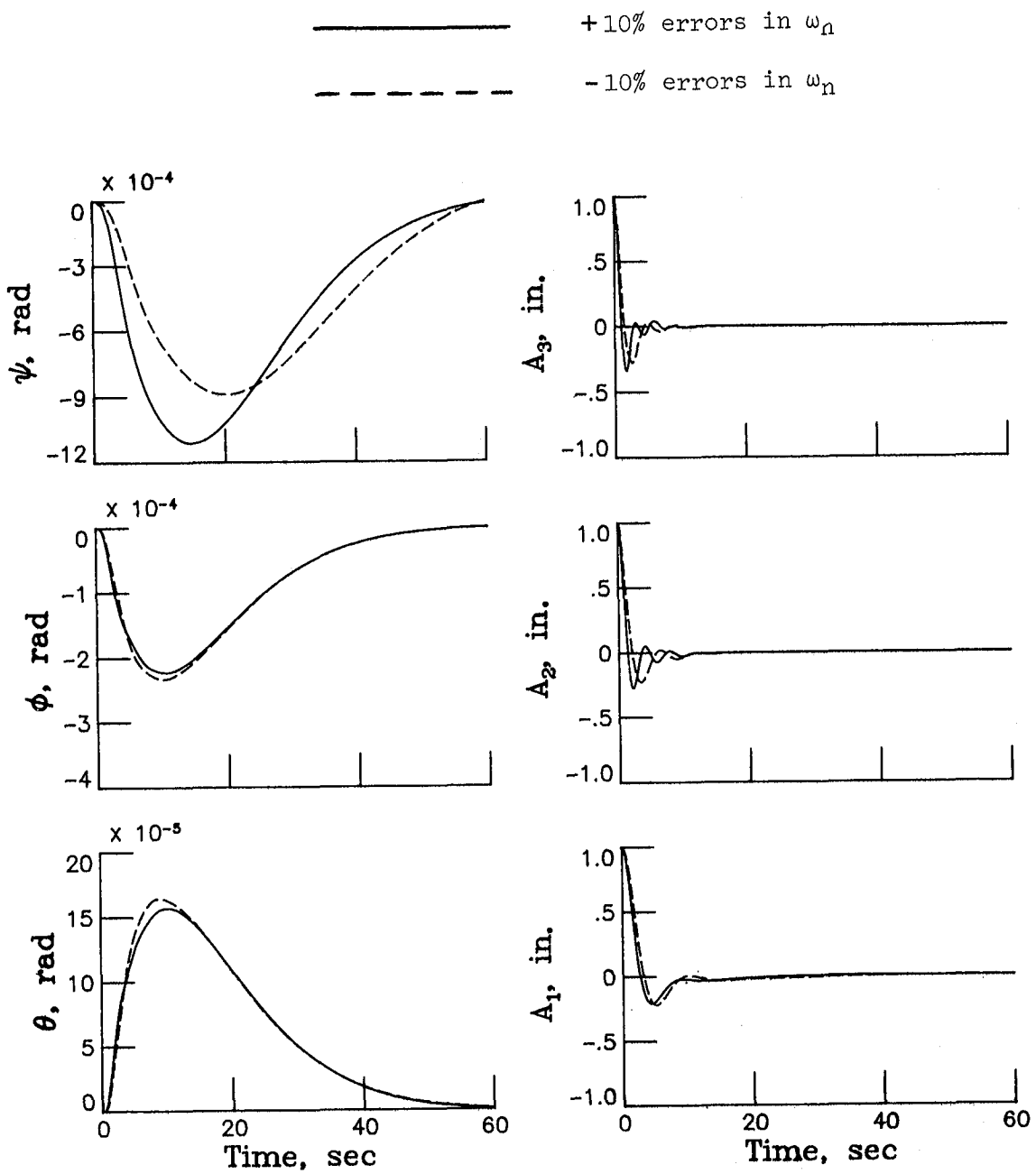

(b) LQR flexible-mode control.

Figure 5. Continued.

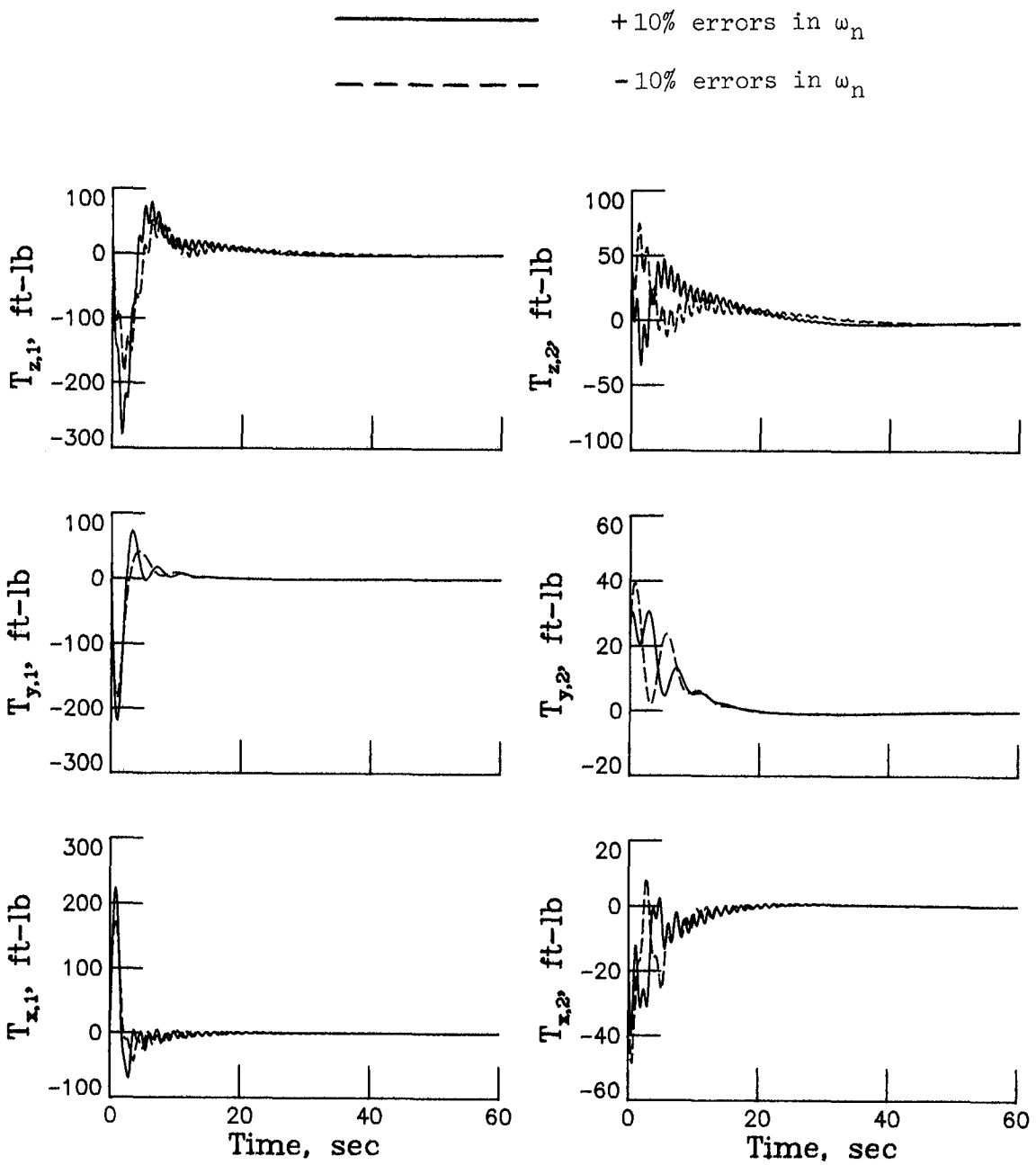

(b) Continued.

Figure 5. Continued.

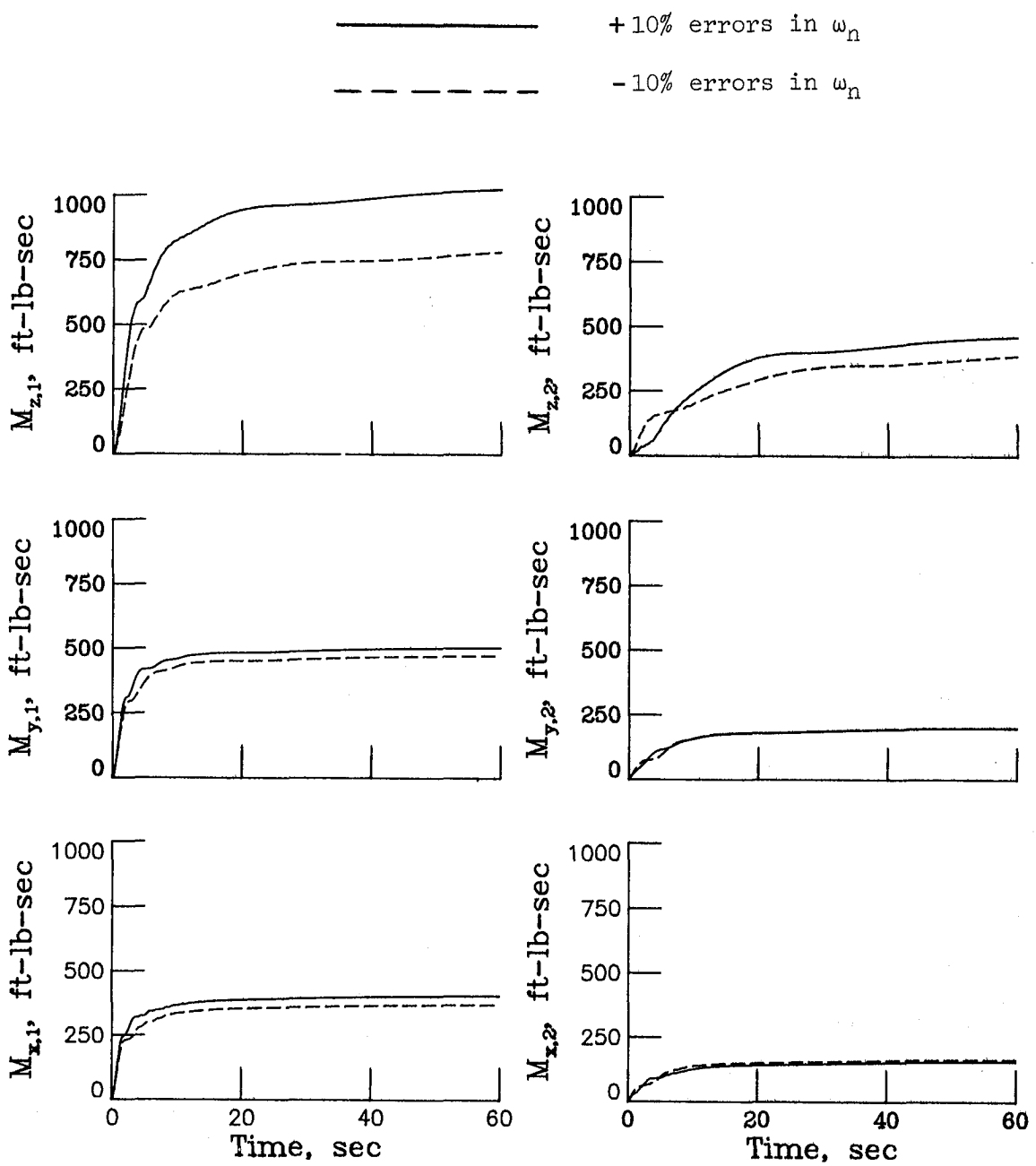

(b) Concluded.

Figure 5. Concluded.

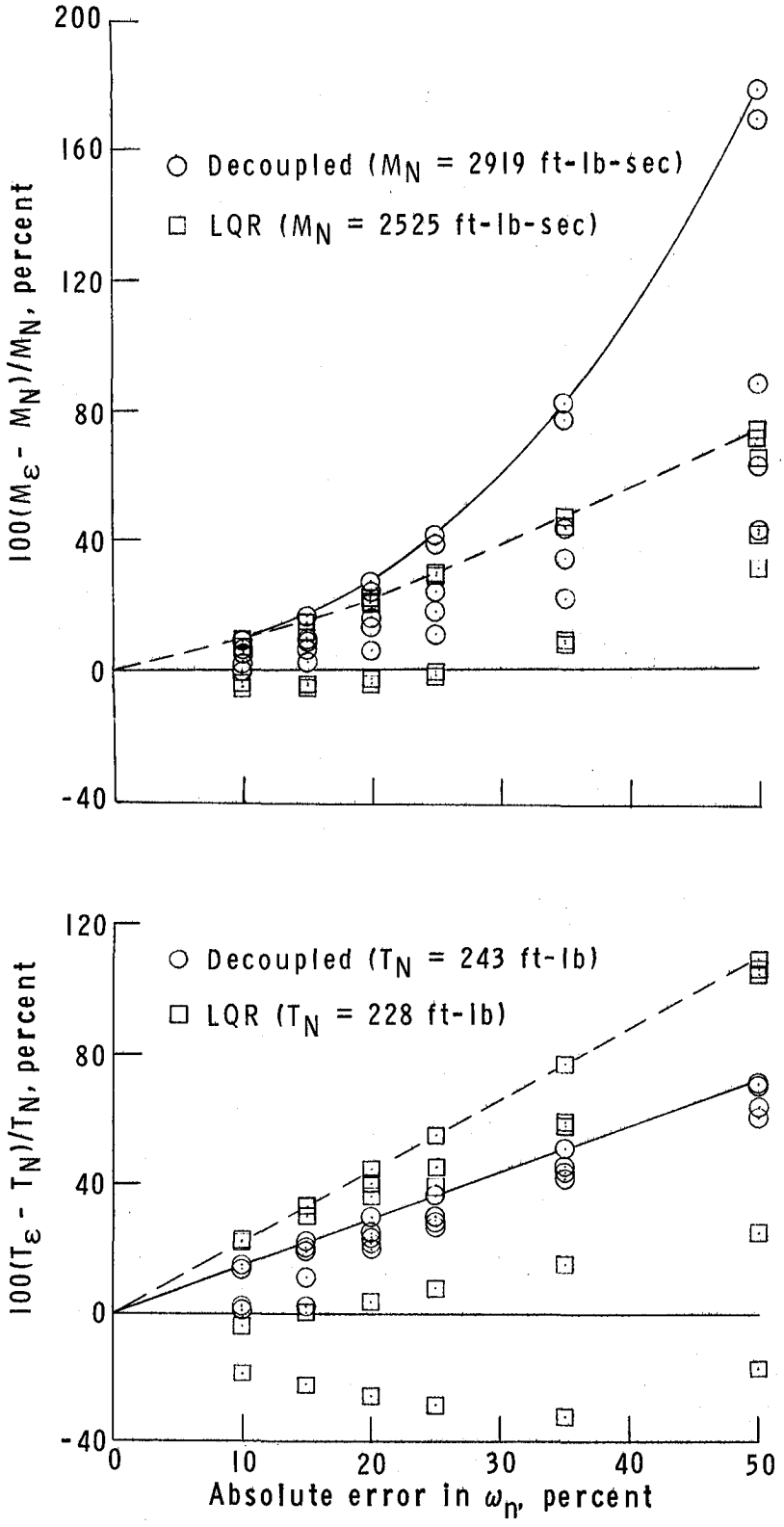

Figure 6. Effect of model frequency error on control requirements for decoupled and LQR flexible-mode control. The solid and dashed curves were faired through the maximum values obtained.

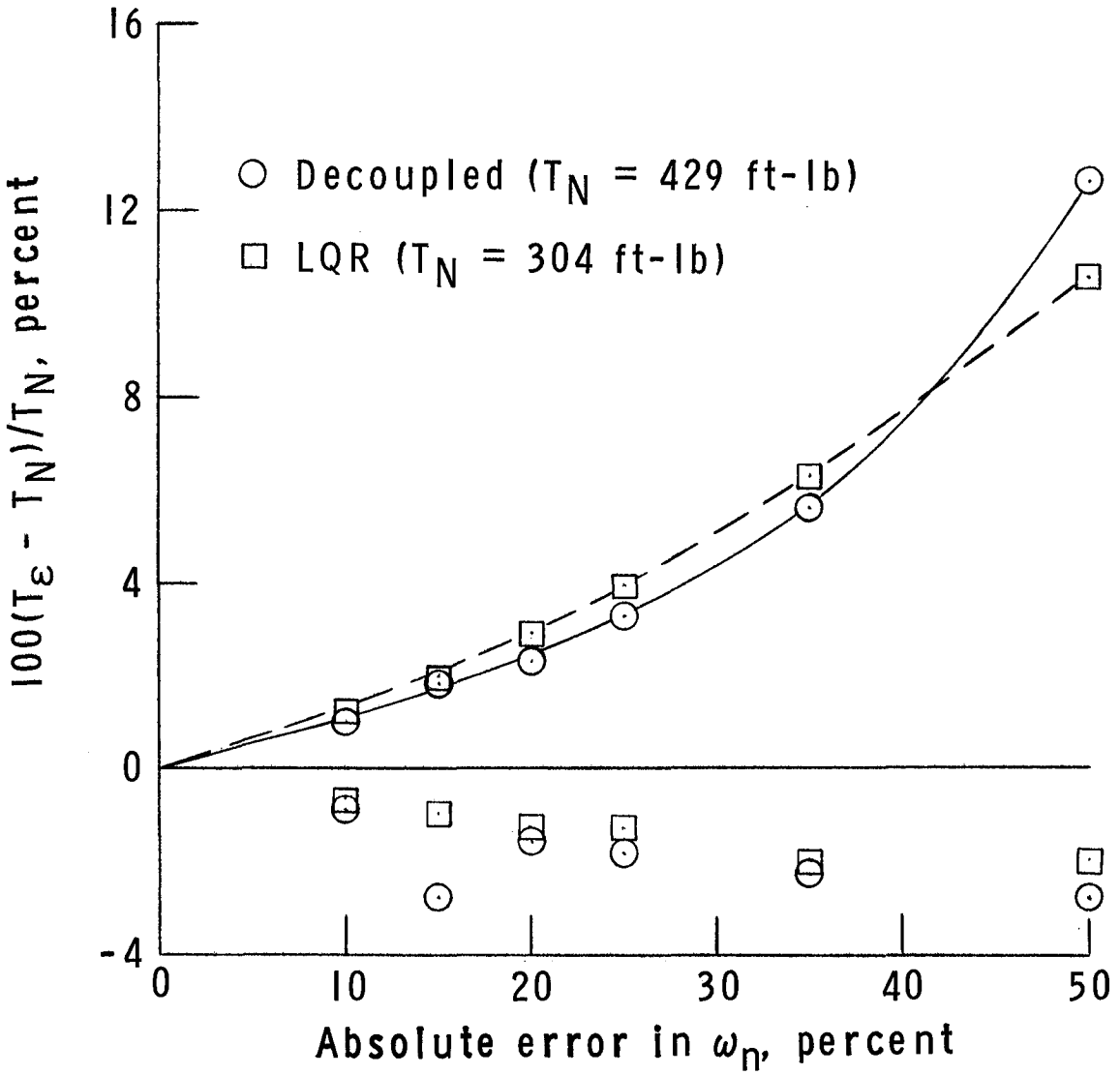

Figure 7. Effect of model frequency error on torque for decoupled and LQR rigid-body control. Only maximum positive and negative changes shown; the solid and dashed curves were faired through the maximum values obtained.

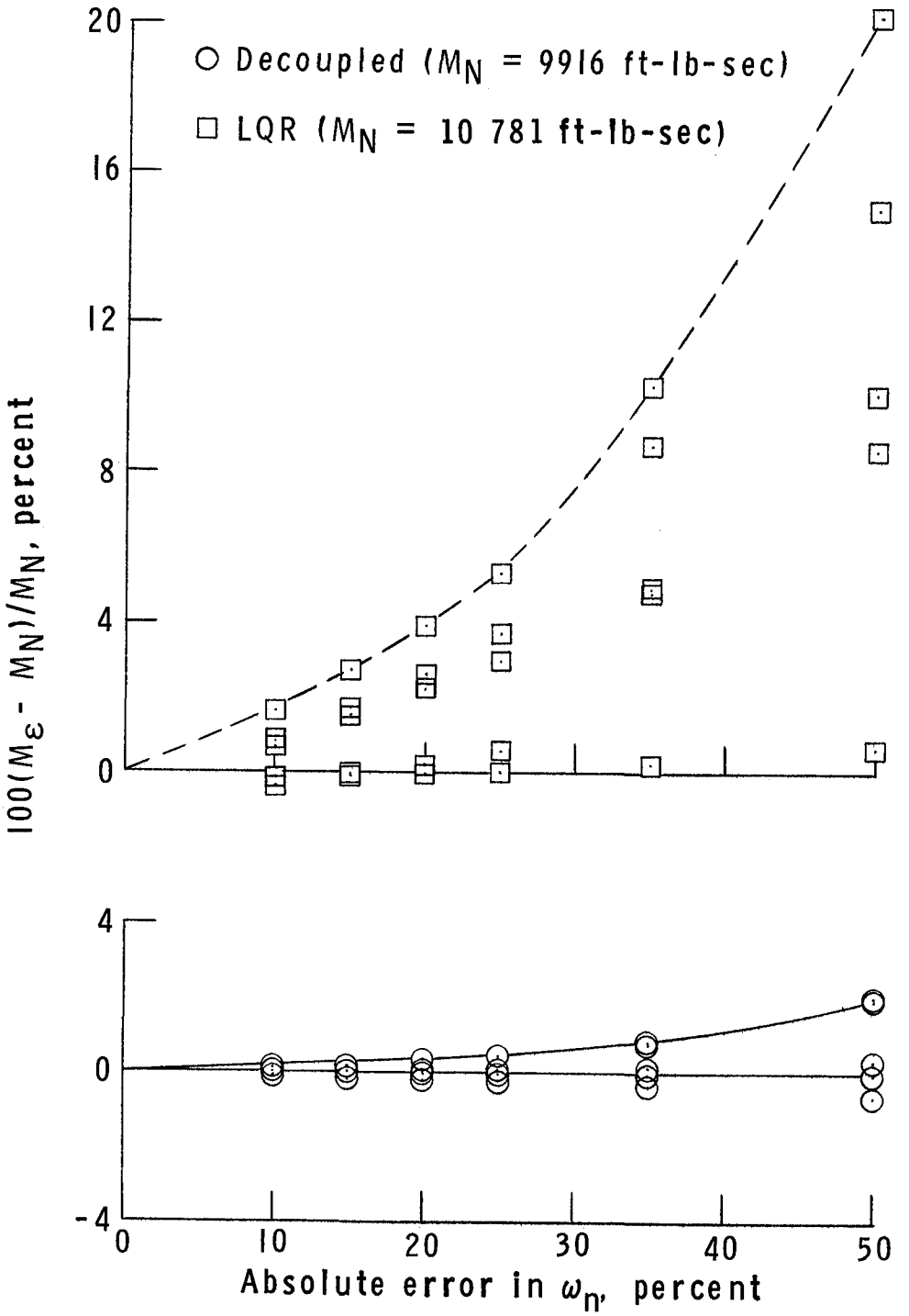

Figure 8. Effect of model frequency error on total momentum for decoupled and LQR rigid-body control. The solid and dashed curves were faired through the maximum values obtained.

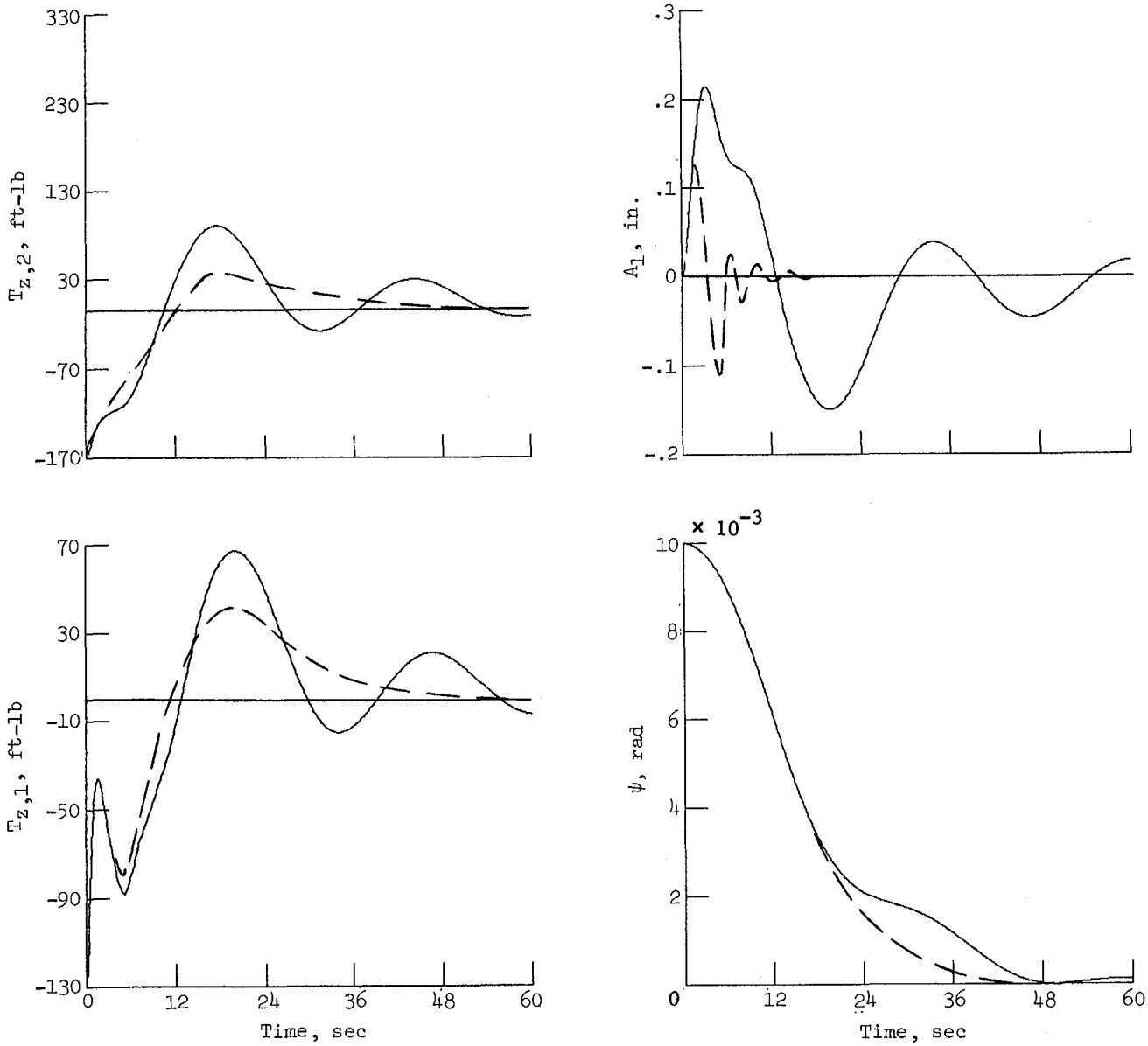

(a) Torque response.

(b) Modal response.

Figure 9. Example of poor performance for LQR rigid-body control using one three-axis attitude sensor at top of antenna column. Error in ω_n, ± 10 percent; dashed curves indicate no-error case.

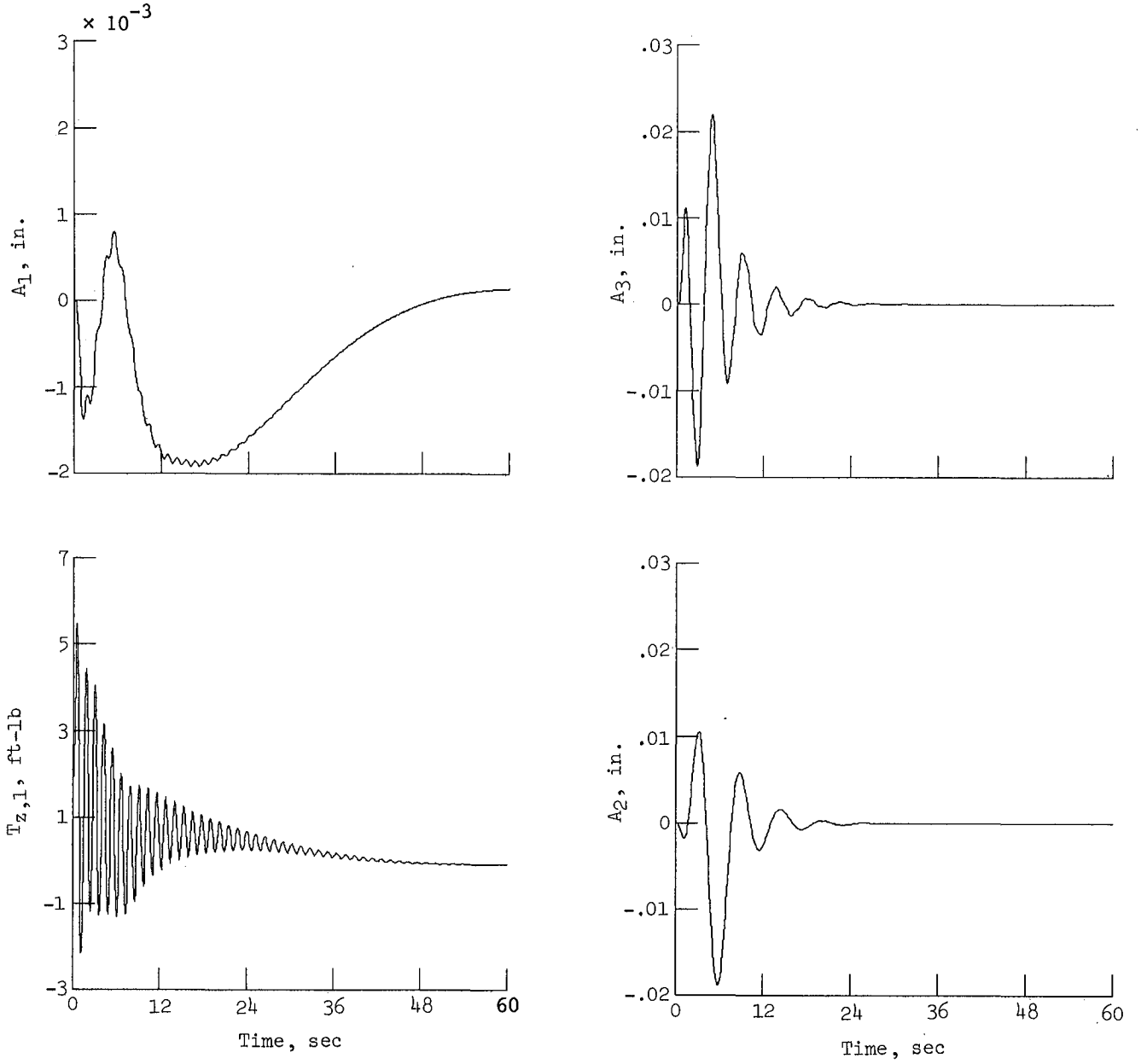

(a) All six control actuators in operation.

Figure 10. Typical responses for decoupled rigid-body control using two three-axis sensors. Error in ω_n, ± 10 percent.

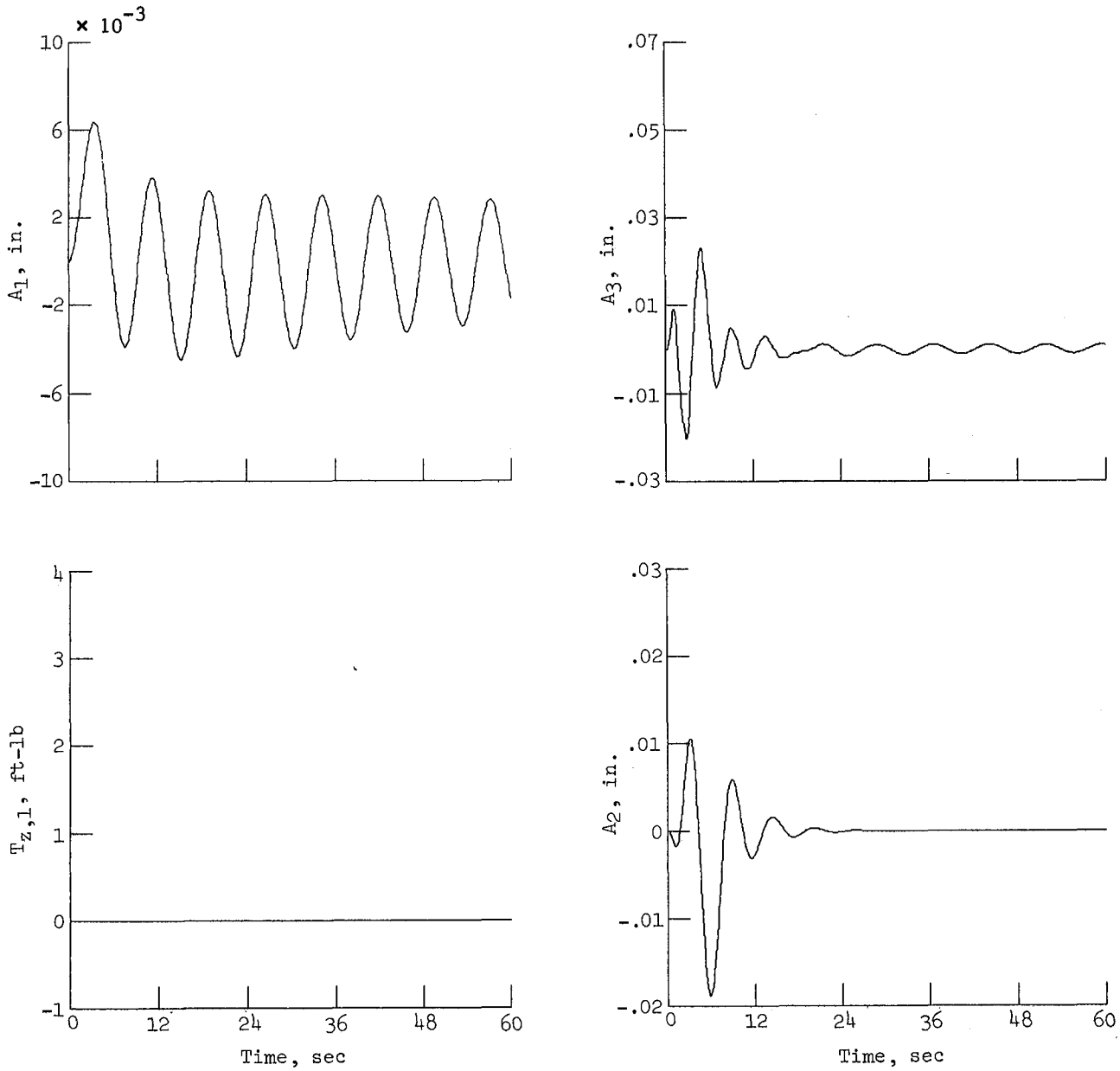

(b) Inoperative z-axis control actuator at top of column.

Figure 10. Concluded.

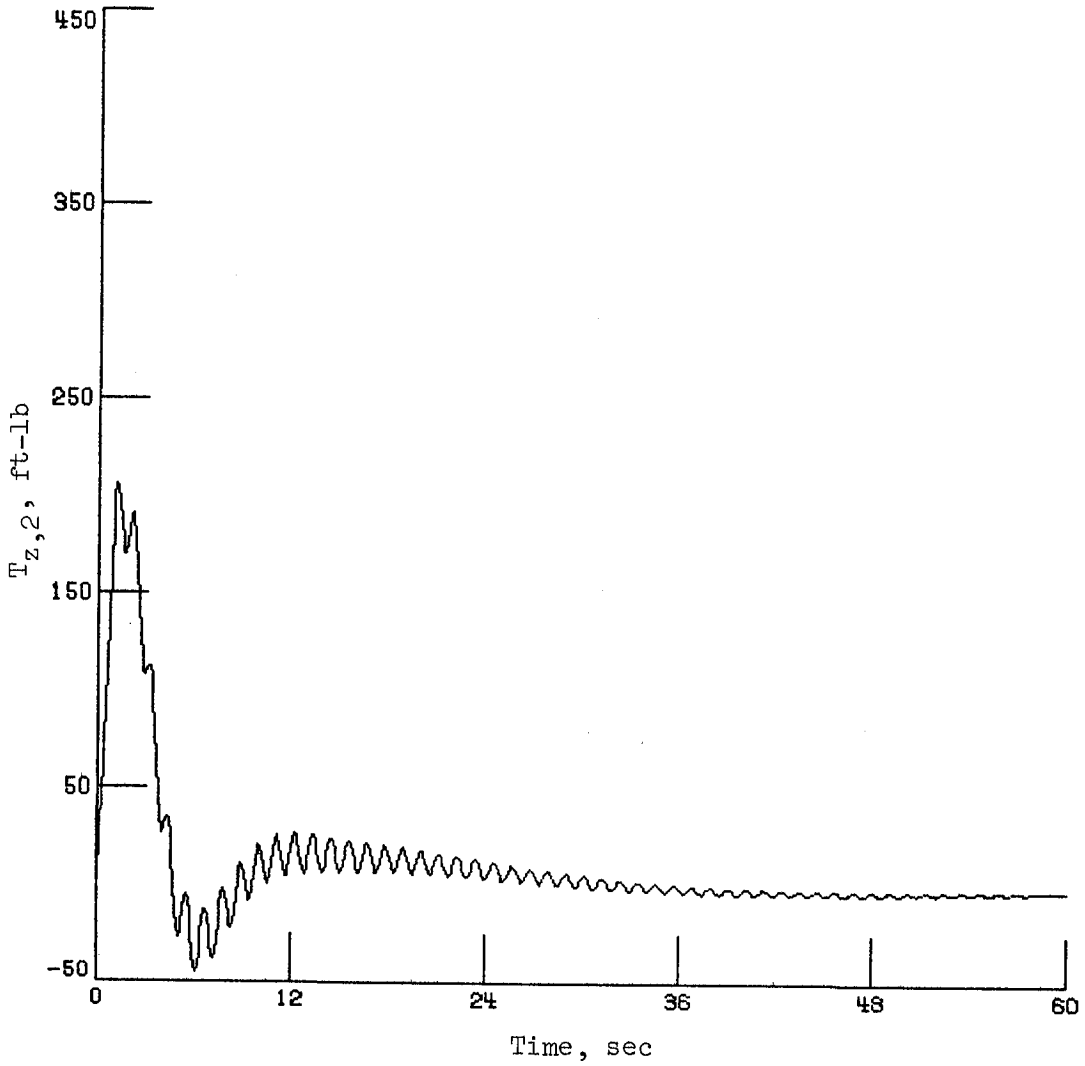

(a) Decoupled control with error in ς_n of -50 percent in all six flexible modes.

Figure 11. Effect of model damping error on z-axis control actuator at bottom of antenna column (location 2) when controlling flexible modes.

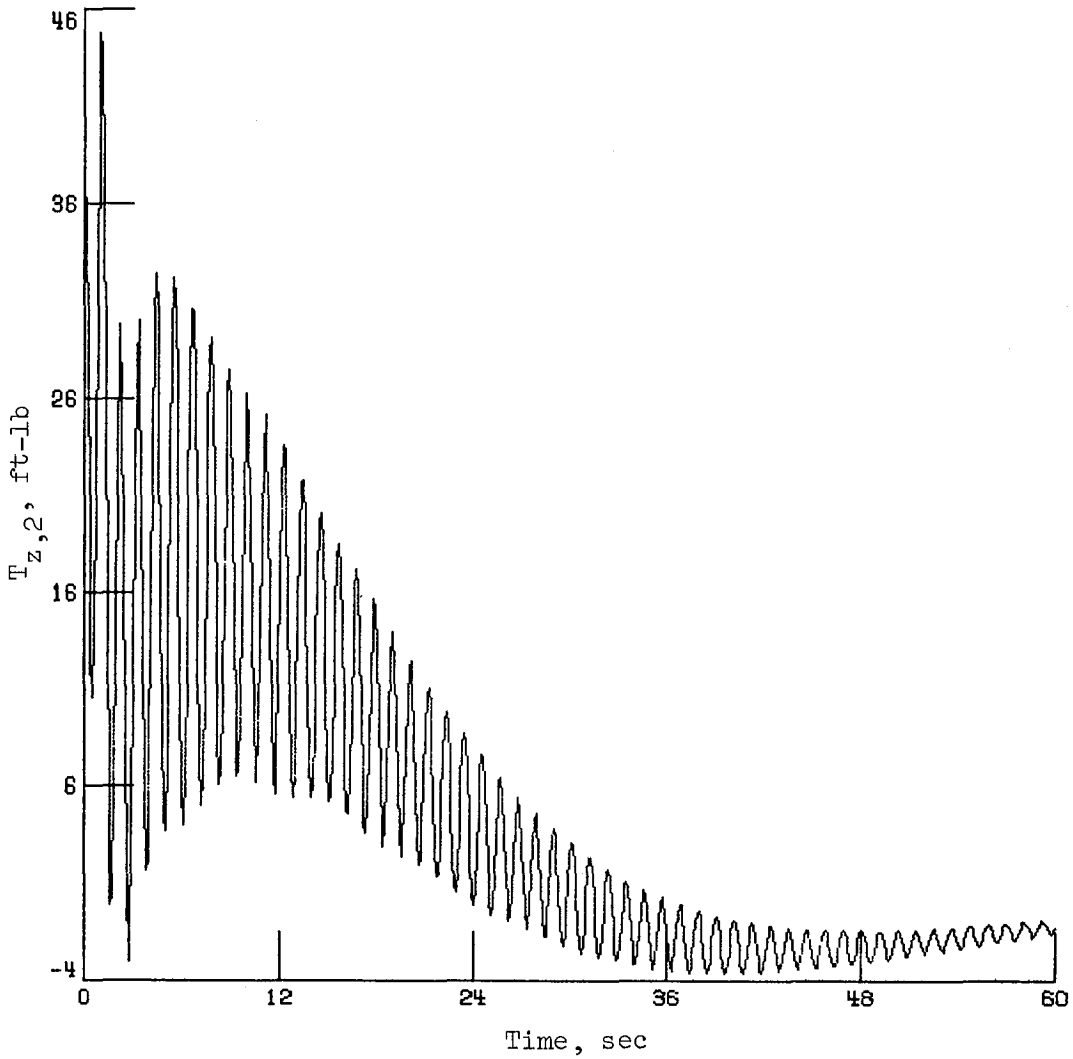

(b) LQR control with error in ς_n of -50 percent in all six flexible modes.

Figure 11. Continued.

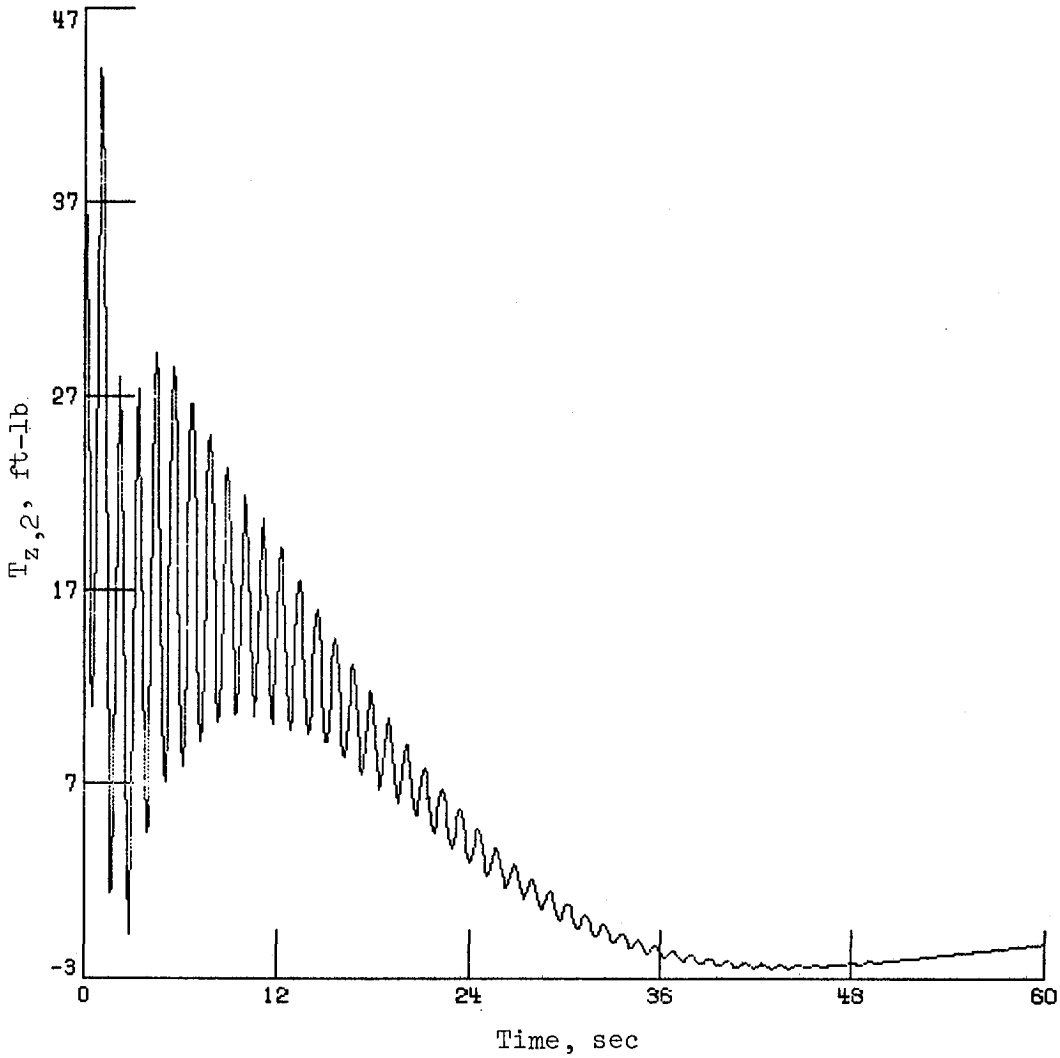

(c) LQR control with error in ς_n of -50 percent in first three flexible modes.

Figure 11. Continued.

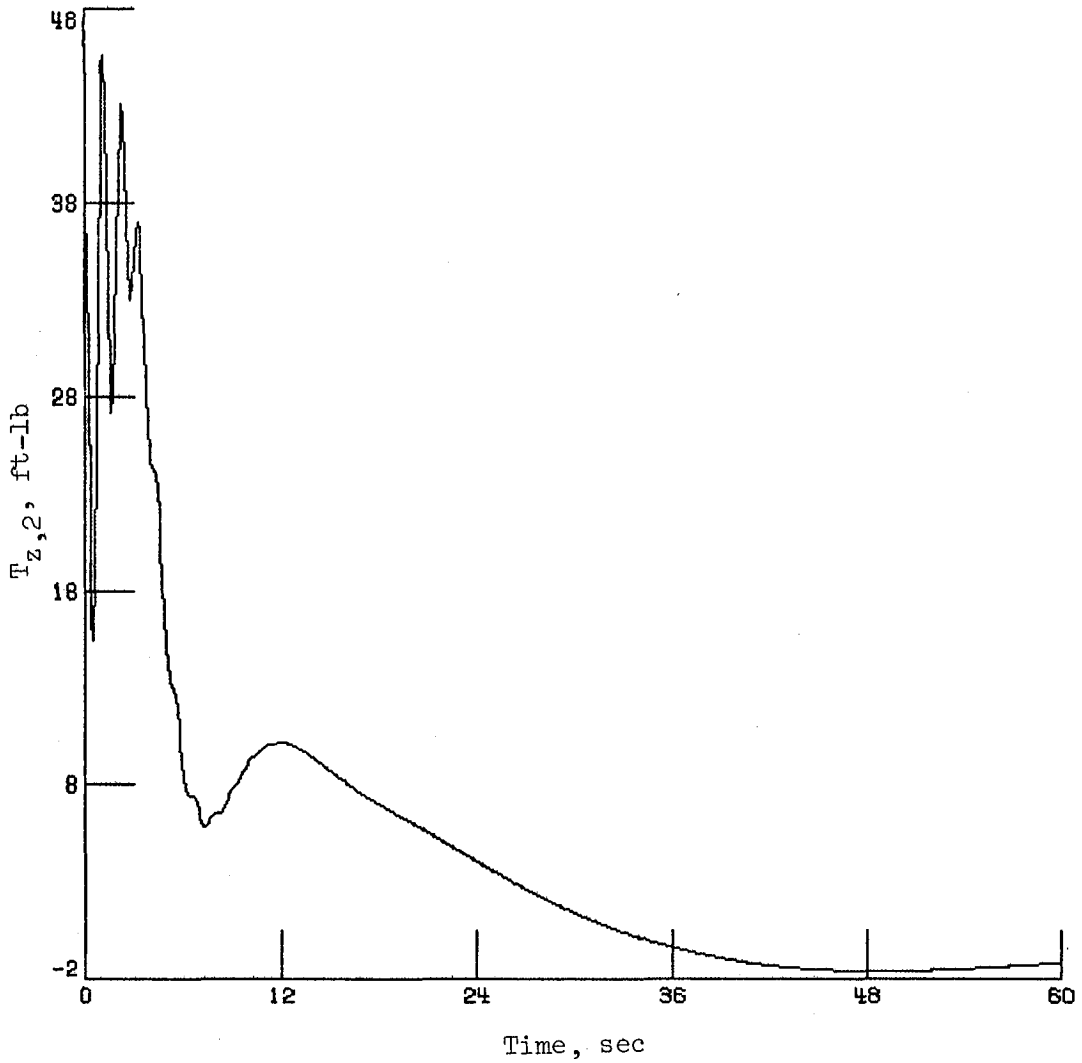

(d) LQR control with error in ζ_n of +900 percent in all six flexible modes.

Figure 11. Concluded.

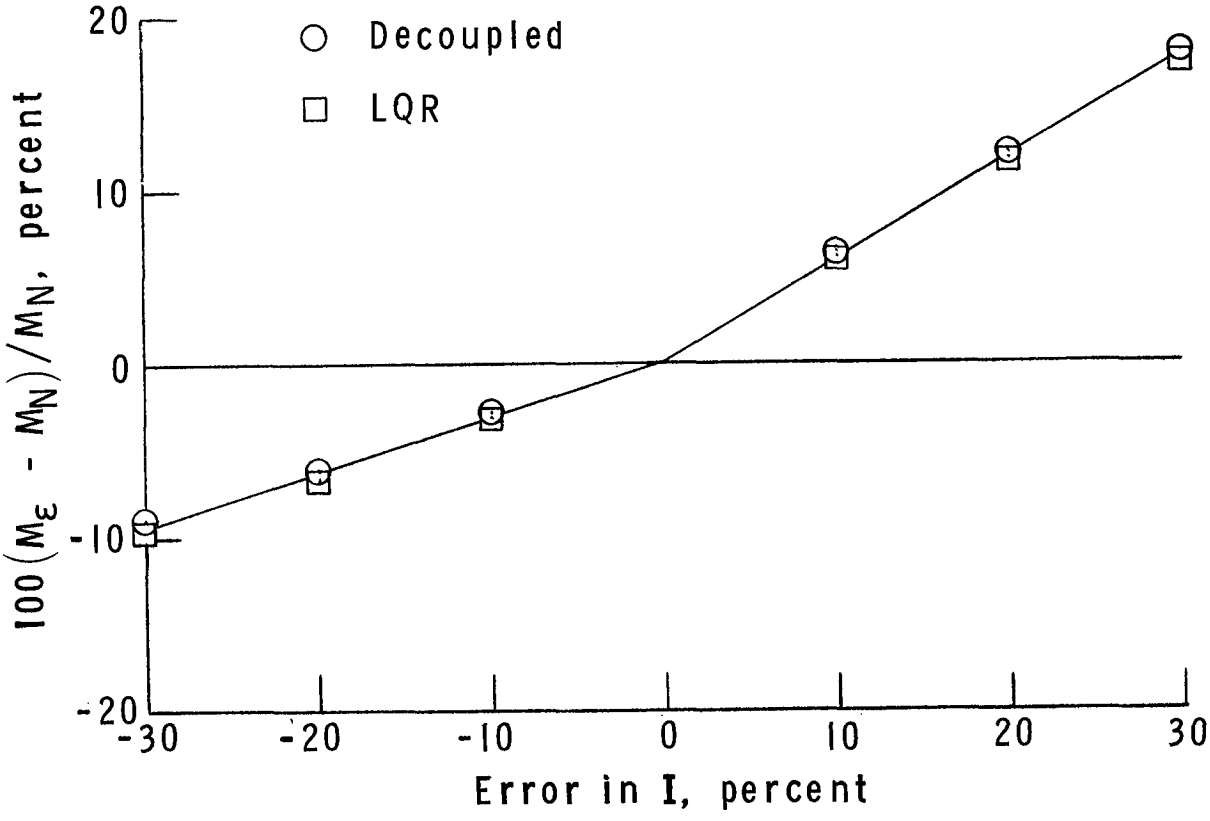

(a) Rigid-body control.

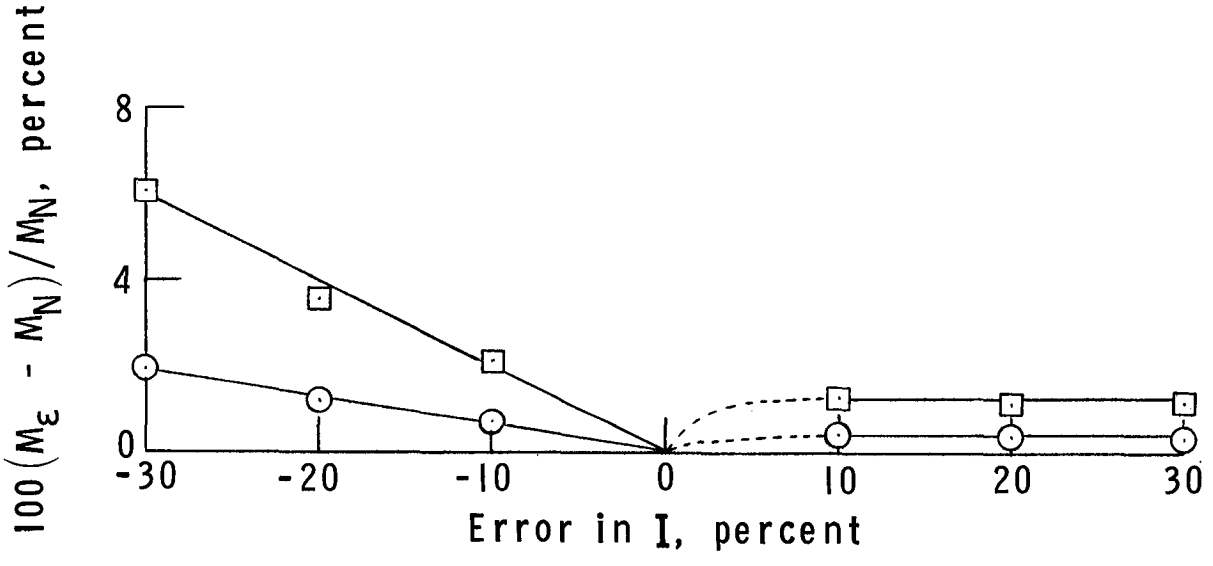

(b) Flexible-mode control.

Figure 12. Effect of model error in I on total momentum for decoupled and LQR control. M_N values given in figures 6 and 8.

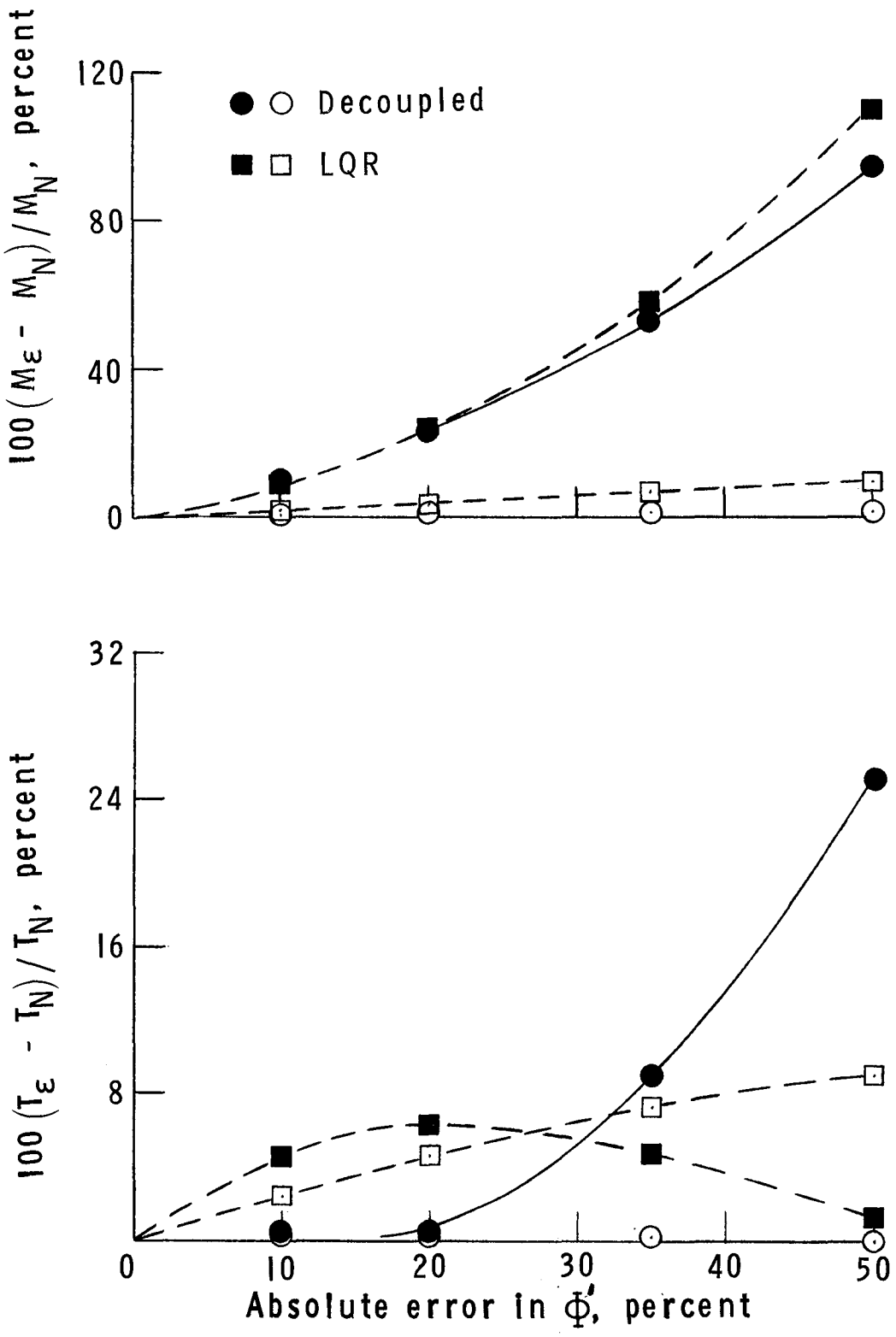

Figure 13. Effect of model error in Φ' on control requirements for decoupled and LQR control. Open symbols denote rigid-body control and solid symbols denote flexible-mode control; T_N and M_N values are given in figures 6, 7, and 8; the solid and dashed curves were faired through the maximum values obtained.

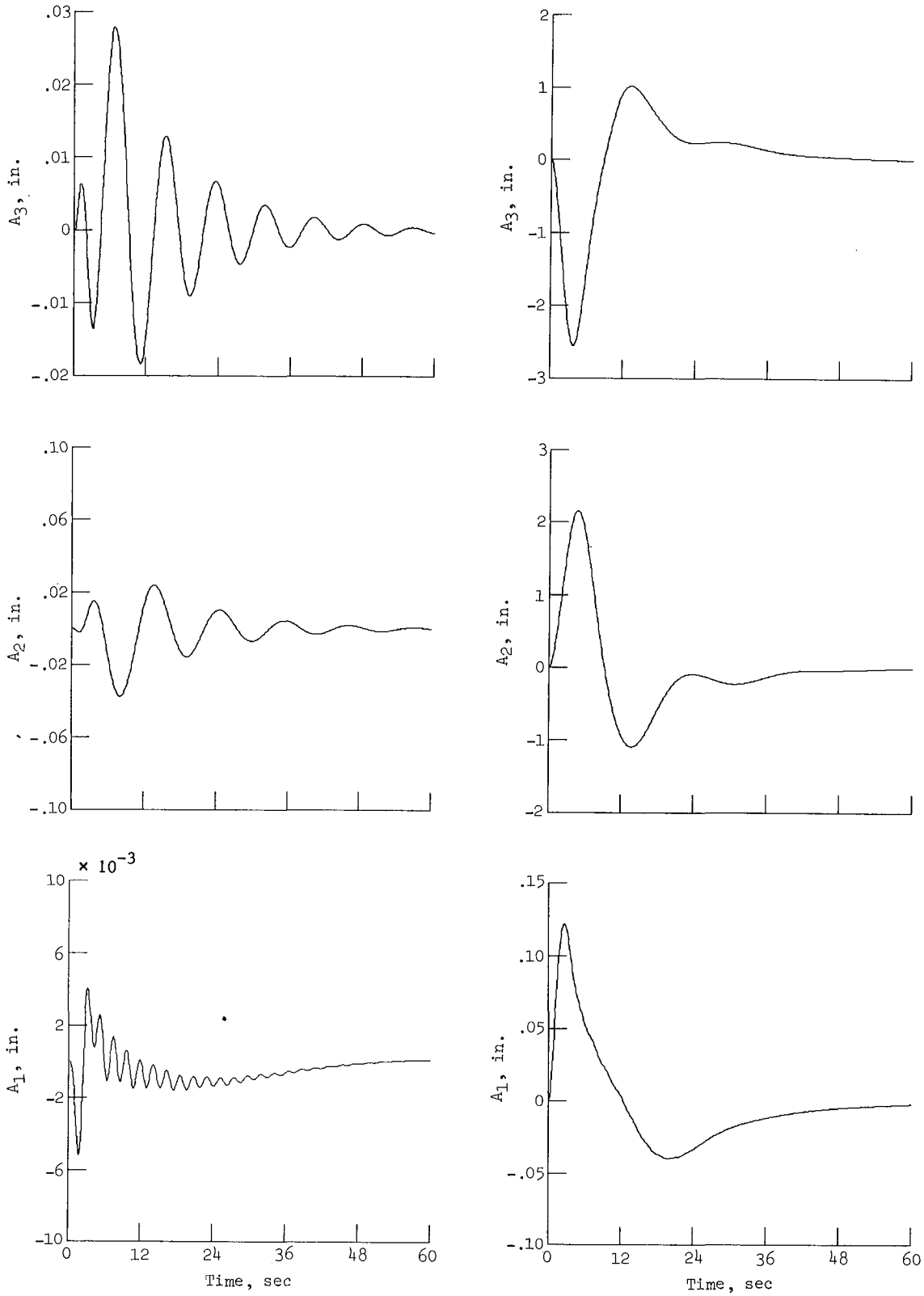

(a) Decoupled control.

(b) LQR control.

Figure 14. Typical transient response for rigid-body control with error in ω_n of ±50 percent.

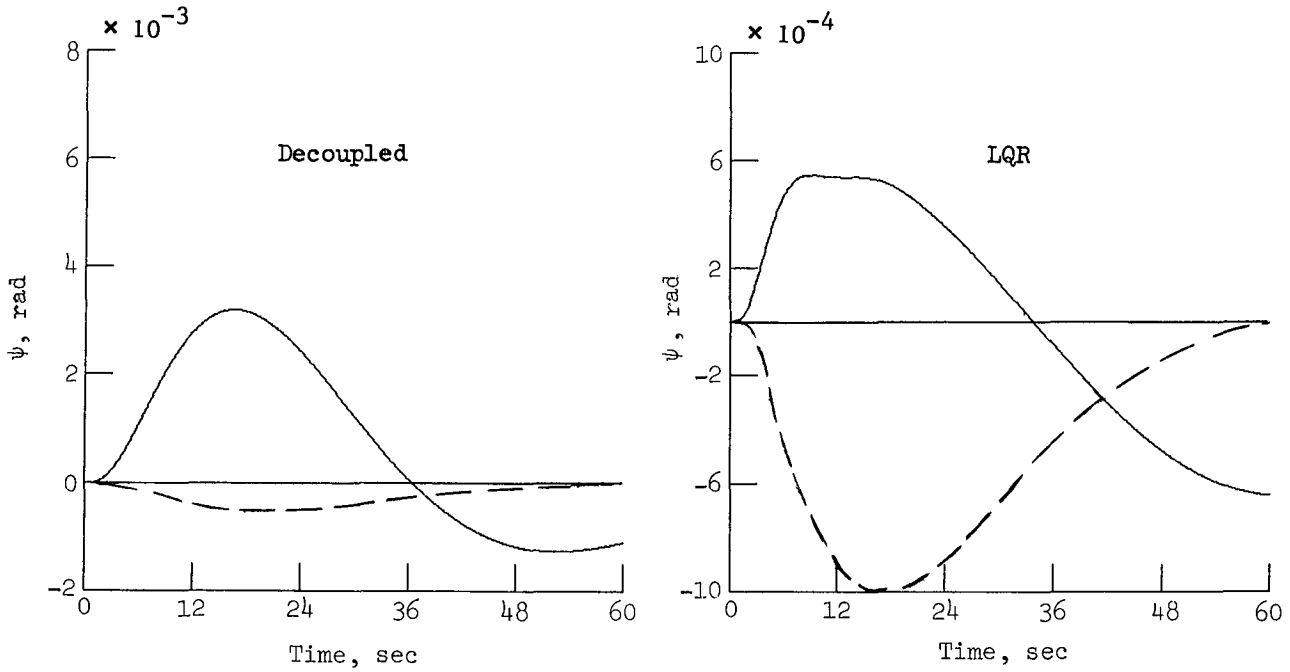

(a) Error in ω_n, −50 percent.

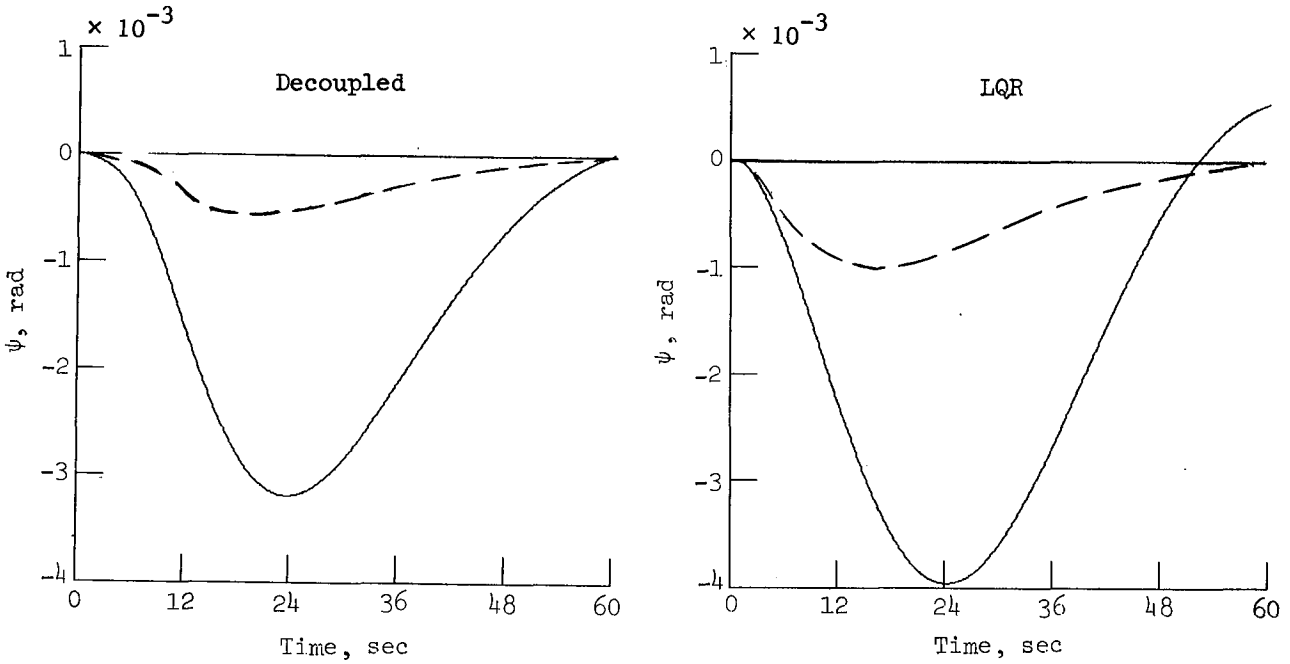

(b) Error in $\mathbf{\Phi}'$, ±50 percent.

Figure 15. Effect of model error on ψ transient during flexible-mode control. Dashed curves indicate no-error case.

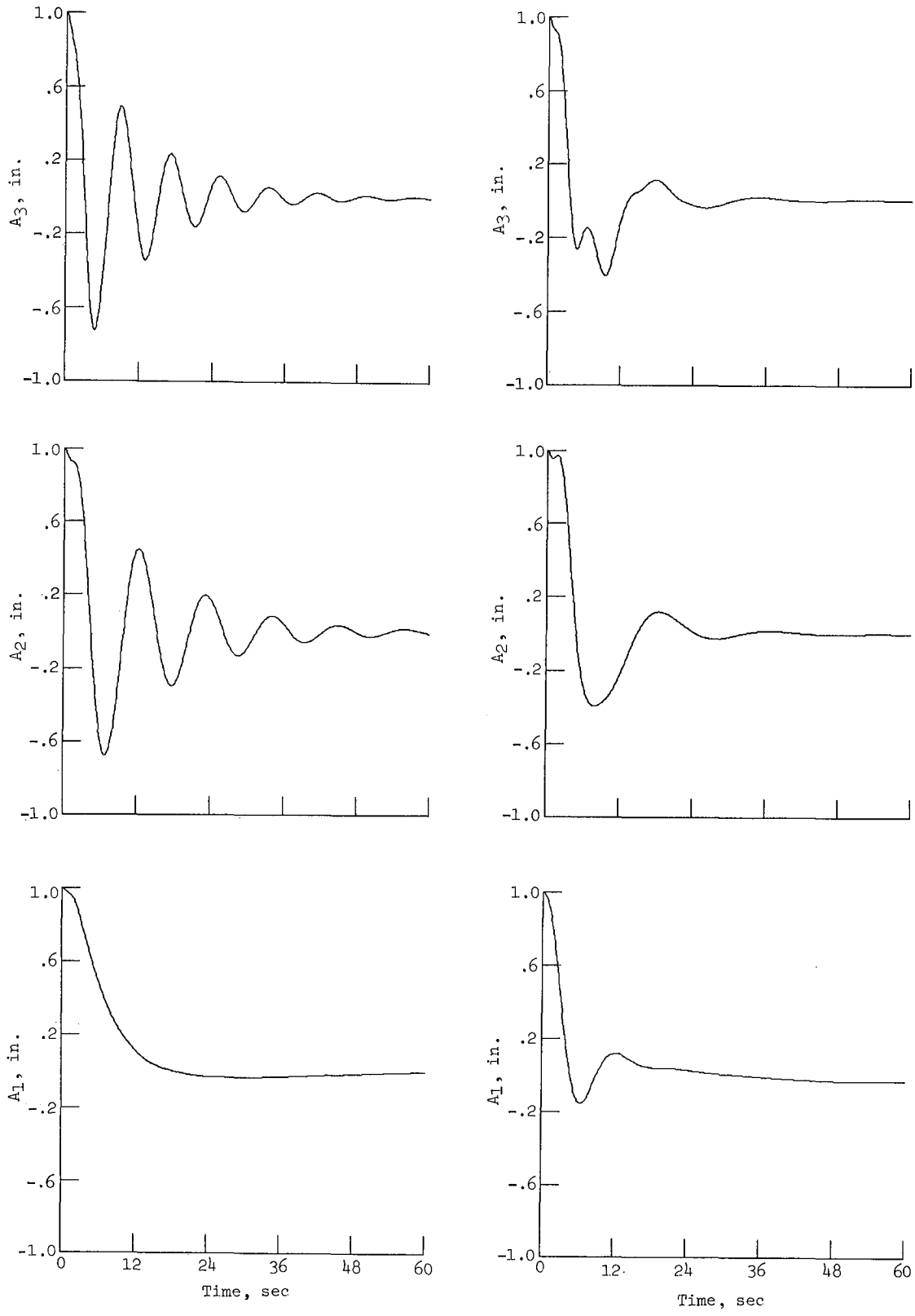

(a) Decoupled control with error in ω_n of −50 percent.

(b) LQR control with error in ω_n of −50 percent.

Figure 16. Effect of model error on time to null for flexible-mode control.

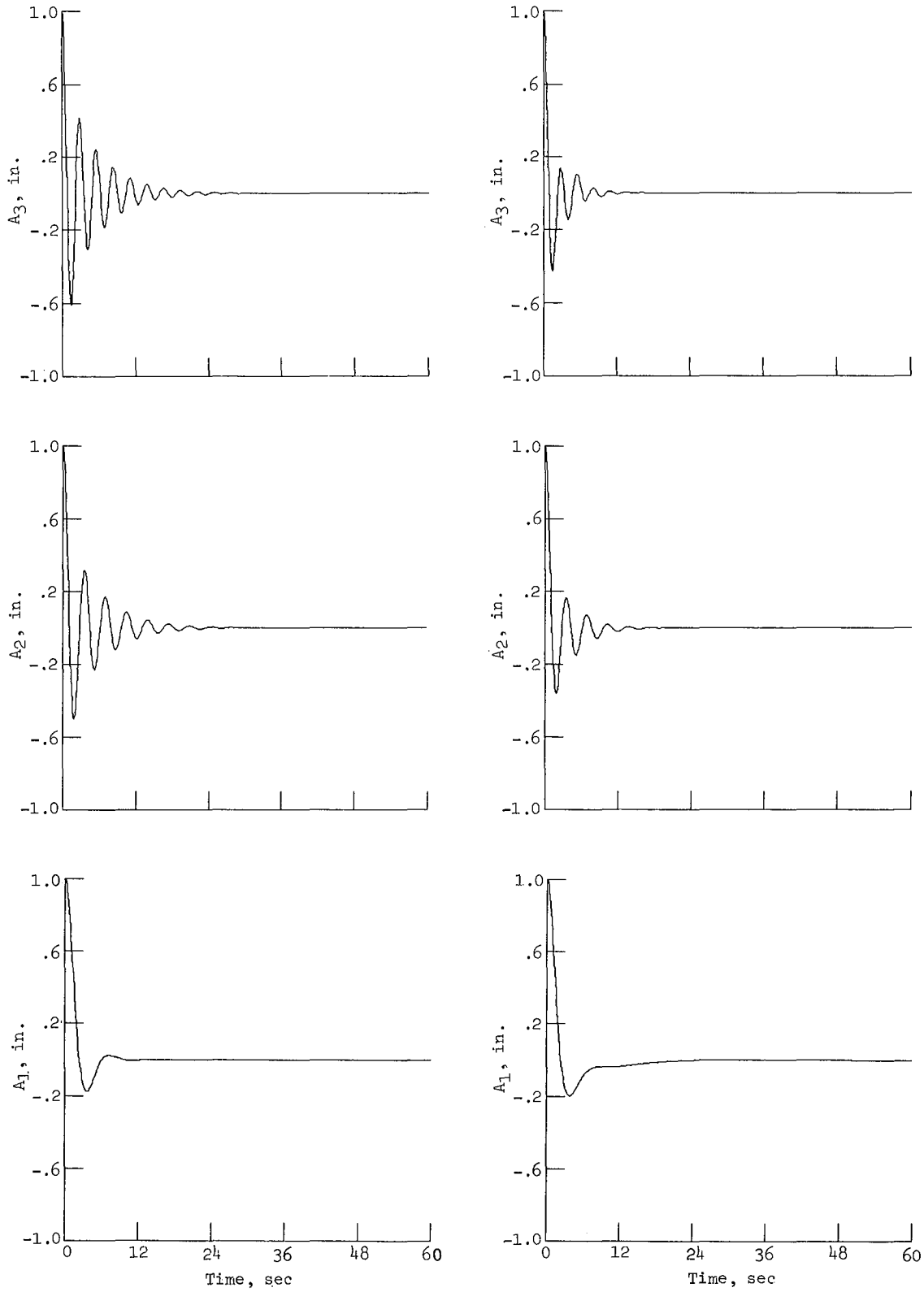

(c) Decoupled control with error in ω_n of ±25 percent.

(d) LQR control with error in ω_n of ±25 percent.

Figure 16. Continued.

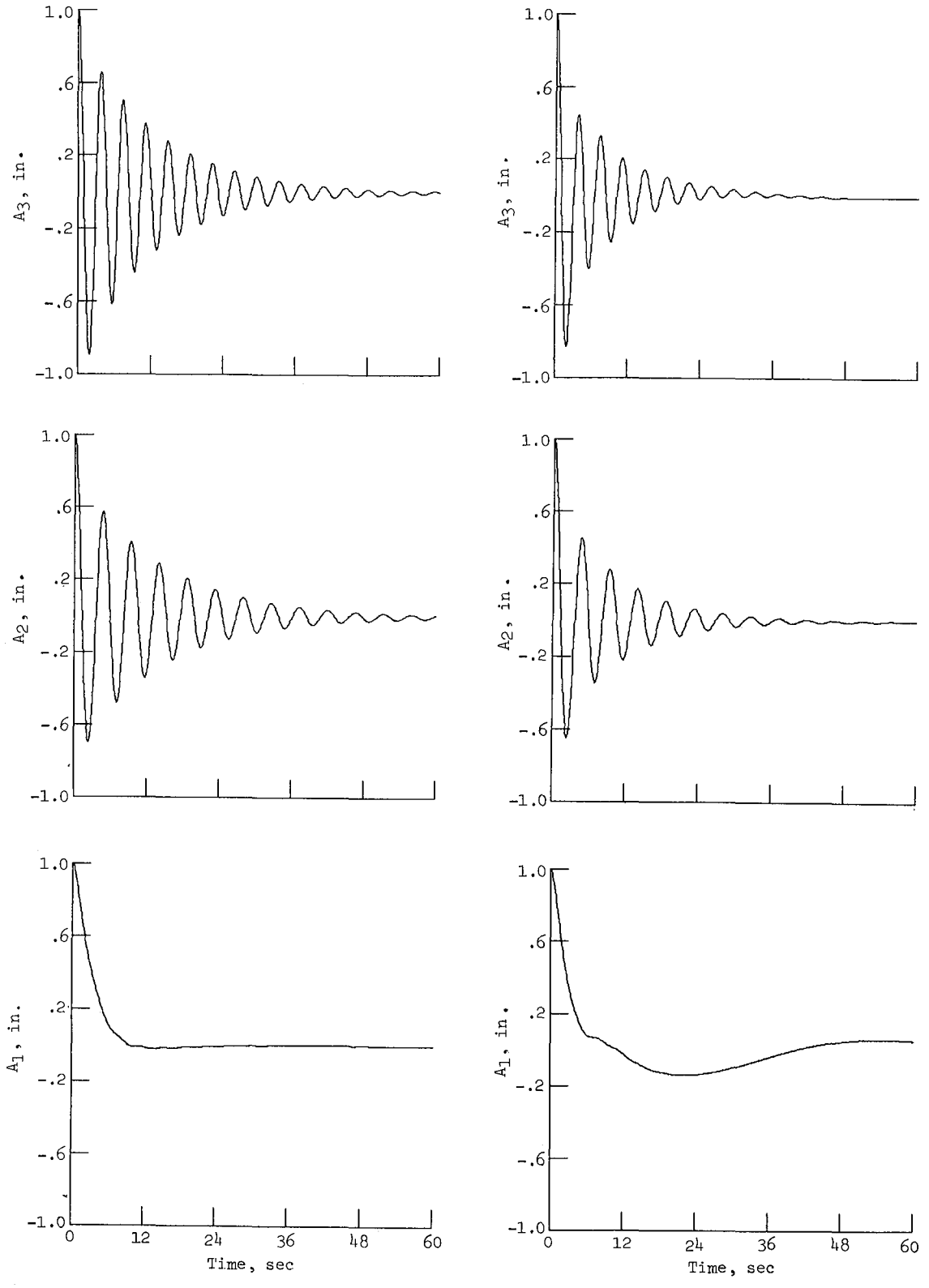

(e) Decoupled control with error in Φ' of ±50 percent.

(f) LQR control with error in Φ' of ±50 percent.

Figure 16. Concluded.

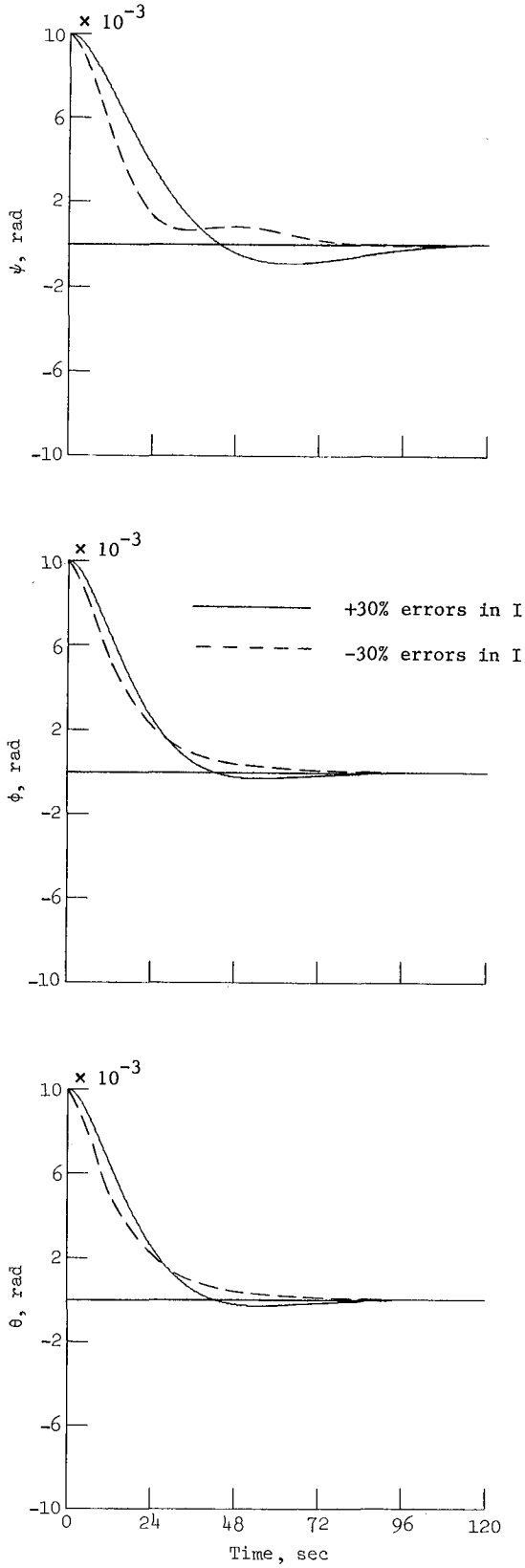

Figure 17. Comparison of responses for two sets of model errors in I using rigid-body control.

Standard Bibliographic Page

1. Report No.	2. Government Accession No.	3. Recipient's Catalog No.
NASA TP-2604		

4. Title and Subtitle	5. Report Date
Effects of Model Error on Control of Large Flexible Space Antenna With Comparisons of Decoupled and Linear Quadratic Regulator Control Procedures	September 1986
	6. Performing Organization Code: 506-46-11-01
7. Author(s): Harold A. Hamer and Katherine G. Johnson	8. Performing Organization Report No.: L-16114
9. Performing Organization Name and Address: NASA Langley Research Center, Hampton, VA 23665-5225	10. Work Unit No.
	11. Contract or Grant No.
12. Sponsoring Agency Name and Address: National Aeronautics and Space Administration, Washington, DC 20546-0001	13. Type of Report and Period Covered: Technical Paper
	14. Sponsoring Agency Code

15. Supplementary Notes

16. Abstract

An analysis has been performed to determine the effects of model error on the control of a large flexible space antenna. Control was achieved by employing two three-axis control-moment gyros (CMG's) located on the antenna column. State variables were estimated by including an observer in the control loop that used attitude and attitude-rate sensors on the column. Errors were assumed to exist in the individual model parameters: modal frequency, modal damping, mode slope (control-influence coefficients), and moment of inertia. Their effects on control-system performance were analyzed either for (1) nulling initial disturbances in the rigid-body modes, or (2) nulling initial disturbances in the first three flexible modes. The study includes the effects on stability, time to null, and control requirements (defined as maximum torque and total momentum), as well as on the accuracy of obtaining initial estimates of the disturbances. The effects on the transients of the undisturbed modes are also included. The results, which are compared for decoupled and linear quadratic regulator (LQR) control procedures, are shown in tabular form, parametric plots, and as sample time histories of modal-amplitude and control responses. Results of the analysis showed that the effects of model errors on the control-system performance were generally comparable for both control procedures. The effect of mode-slope error was the most serious of all model errors.

17. Key Words (Suggested by Authors(s))	18. Distribution Statement
Decoupling Large space structures Linear quadratic regulator Modal control	Unclassified—Unlimited Subject Category 18

19. Security Classif.(of this report)	20. Security Classif.(of this page)	21. No. of Pages	22. Price
Unclassified	Unclassified	50	A03

For sale by the National Technical Information Service, Springfield, Virginia 22161

NASA-Langley, 1986

National Aeronautics and
Space Administration
Code NIT-4

Washington, D.C.
20546-0001